Computer Aided Software Design (CASD) for Light Emitting Diode Modeling

Hla Myo Tun[1]

Abstract

This paper is emphasized on the analysis of computer aided software design for light emitting diode modeling in relation with the electronic properties and band diagram design. As the electronic properties, the current-voltage characteristics, the band-gap energy as a function of temperature, the temperature dependence of emission intensity are described briefly in this research work. The properties and associated characteristics of the materials are analyzed with the result figures. On the other hand, for the band structure design, the research is emphasized by the homostructure and heterostructure of not only the existing known materials but also the other new materials. The band-diagram results are approved by the parameters of the materials such as doping concentrations, effective mass of the materials and so on. The most fundamental materials are silicon and germanium. Beside the silicon and germanium, the band structure also shows the other new materials such as ZnO, ZnCdO, $CsPbBr_3$ and so on. This research will help the researchers who analyze the light emitting diodes.

Keywords: Computer Aided Software Design, Light Emitting Diodes Modeling, MATLAB, Semiconductor Electronics, Computer Software

1. Introduction

The research is emphasized by using computer-based simulation for light emitting diode modeling. The research trend is to find the new device by using simulation tools like MATLAB, the characteristics of proposed devices from analysis, and the calculations of the specifications such as current, voltage of the device in relation with parameters such as temperature. The result is the data of program and the expected output is achieved by changing the parameters. The research includes the most suitable parameters for a device fabrication and the recommendations if this parameter works on such device or not. Nowadays, the use of LED is very widespread, not only for lighting but also in other fields. LEDs present many advantages over incandescent light sources including lower energy consumption, longer lifetime, improved robustness, smaller size, and faster switching. LEDs can produce sufficient light with very smaller power than the traditional light bulbs or fluorescent tubes. For example, crops are successfully grown in downtown warehouse without soil and sun by using LED grow light. In these days, light emitting diodes could soon be the light of the world. Light emitting diodes are made using p-n junction. LED is a two lead

[1] Department of Electronic Engineering, Yangon Technological University, Gyogone Yangon Region, Republic of the Union of Myanmar

semiconductor light source which converts electrical signal into optical signal, when it is operated in forward biased direction. A light-emitting diode (LED) is also a semiconductor light source.

When the junction is forward biased, electrons and holes are injected in the opposite directions across the junction's depletion region. As these injected holes and electrons recombine with electrons and holes on the n and p sides of the junction, light is emitted in the form of photons. Thus among the four kinds of luminescence, namely photoluminescence (PL), cathodoluminescence (CL), electroluminescence (EL), radioluminescence (RL), light-emitting diode works for the electroluminescence effect and the color of the light is determined by the energy gap of the semiconductor. The optimization of the device design is usually done by computer simulation, and this must be based upon the physical processes which actually occur in the devices and must use appropriate values for material parameters. Simulations agree well with experimental data for diode current as a function of temperature for a variety of device structures. A comprehensive temperature analysis of the LED devices is performed based on the temperature dependencies of the physical parameters [1].

The research includes the comparison of electrical and optical characteristics, the temperature dependence of emission intensity, the band gap energy as a function of temperature, the voltage-current (V-I) characteristics, with a reference of LED. In this research, the results of a self-consistent numerical simulation of light emitting diodes could be confirmed by experimental results. All material parameters based on recent literature values as well as our own experimental data are evaluated. However, experimental data does not exist for many material parameters in these simulations and reasonable estimations have to be used. Simulations using the programs provided the opportunity to study the effect of different device parameters on the overall device performance. The performance of the device was improved until an optimal device configuration was created for a particular application [2].

This research work is done on computer-based simulation for light emitting diode modeling. The researchers who analyze light emitting diodes are making experiments practically. Then, after the experiments, results are proved right by the theoretical point of view. Since this method is experiment dependant and the experiment is not affordable, it will not be worked.

For that condition, computer simulation will be a great assistance. So, computer-based method is the most appropriate method. Based on not very few amounts of characteristic equations, the associated characteristic curves are drawn in this paper. As the band-gap structures vary, the operating principals done by the light emitting diodes vary. They are not the same. These facts which are based on the development of computer-based simulation design for LED modeling are all gathered in this paper.

The research is to find out the most suitable parameters for a device. The research includes simulation the program using equations which are derived from existing system of literature background and the characteristic curves and the recommendation whether this parameter works on such device or not. The algorithms are implemented by using MATLAB programming. And the performance of the proposed system is evaluated and compared the results with the associated properties.

2. Light Emitting Diode

A light emitting diode (LED) is a two-lead semiconductor light source. It is a p-n junction diode, which converts electrical signal into optical signal. When the junction is forward biased, electrons and holes are injected in opposite directions across the junction's depletion region. As these injected holes and electrons recombine with electrons and holes on the n and p sides of the junction, light is emitted from the diode in the form of photons. LED is a p-n junction opto-semiconductor that emits a monochromatic (single color) light when operated in a forward biased direction. When p-n diode is forward biased, annihilation of holes and electrons takes place close to the junction and some energy is released in the junction. In Ge, Si, this energy is in the form of heat. In GaAs (gallium arsenide), the energy is released in the form of radiation. This phenomenon is known as electro-luminescence and the diode based upon this phenomenon is called LED. When a suitable voltage is applied to the leads, electrons are able to recombine with electron holes within the device, releasing energy in the form of photons. Electroluminescence can be defined as the emission of light from a semiconductor under the influence of an electric field. The color of the light is determined by the energy band gap of the semiconductor. The wavelength of the light emitted, and thus its color, depends on the band gap energy of the materials forming the p-n junction. Band gap refers to the energy difference (eV) between the top of the valence band and the bottom of the conduction band in insulators and semiconductors LED is capable of emitting a fairly narrow bandwidth of visible or invisible light when its internal diode junction attains a forward electric current or voltage. LEDs are of two kinds: visible and invisible colors. The visible lights that an LED emits are orange, red, yellow, or green. The invisible light includes the infrared light. Red is the most common color among them. The differences in the LED colors are due to the differences in the semiconductor substrate material such as gallium arsenide, gallium arsenide phosphide and the associated wavelength. LED denotes high power, good efficiency and faster response time of 0.1μs. LED technology has now developed to the point where there are several different types of LED. Light emitting diodes are one of the fastest growing sectors in the electronic component industry. Applications of light emitting diode are sensor applications, mobile applications, sign applications, LED signals, indicators, traffic light, barcode scanner, LED street lights, LED lamps, LED displays, LED car brake lights and so many other electronic things.

3. Generation and Recombination in Semiconductors

Quantum mechanics is the science of the very small. Quantum mechanics is also the body of scientific laws that describe the behavior of photons, electrons and the other particles that make up the universe. A quantum-mechanical approach can be taken using the time-dependent perturbation theory, Fermi's golden rule. In general, these generation-recombination processes can be classified as radiative or non-radiative. The radiative transitions involve the creation or annihilation of photons. The non-radiative transitions do not involve photons. They may involve the interaction with phonons or the exchange of energy and momentum with another electron or hole. The generation rate is

$G_n = G_p = e$, e is an emission rate.

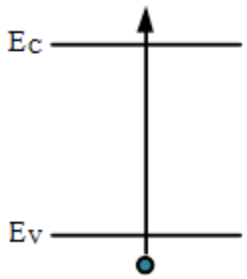

Figure 1 Energy Band Diagram for Generation of an Electron-Hole Pair

For the recombination of electron-hole pair, the recombination rate is

$R_n = R_p = cnp$ where c is the capture coefficient.

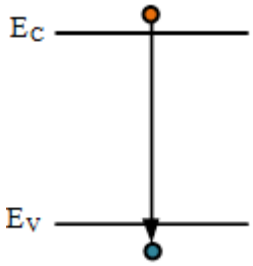

Figure 2 Energy Band Diagram for Recombination of Electron-Hole Pair

The net recombination rate is given as follows.

$R = R_n - G_n = R_p - G_p = cnp - e$

4. Radiative and Non-radiative Recombination

Electrons and hole recombine either radiatively or non-radiatively. However, radiative recombination is clearly a preferred process because it emits light emission. There are three bands to measure the electronic band-gap; the conduction band, valence band and the interband. So, the laser excitation excited the semiconductor sample. At this condition, the recombination process takes place. Electrons only recombine with holes that have the same momentum. Electrons and holes in semiconductors recombine either radiatively or non-radiatively [3].

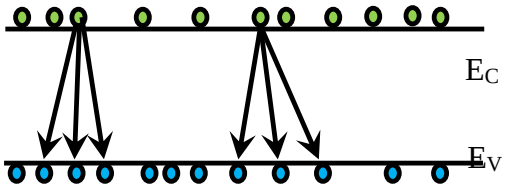

Figure 3 Illustration of Electron-Hole Recombination [3]

5. Radiative Electron-Hole Recombination

Radiative recombination is clearly the better process than non-radiative recombination. Radiative recombination results in light emission. During radiative recombination, electron and holes recombine with each other and light is emitted in the form of photons [4].

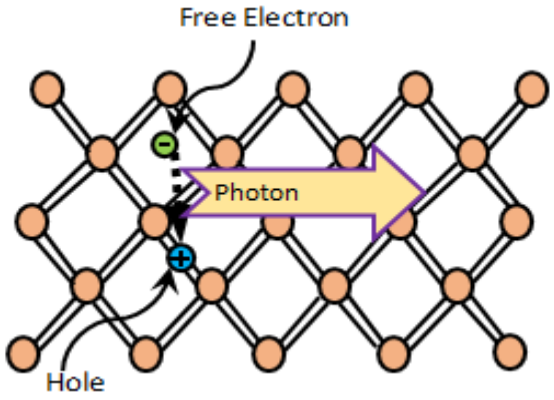

Figure 4 Radiative Recombination of an Electron-Hole Pair Accompanied by the Emission a Photon with Energy hv=Eg [4]

There are two types of free carriers, namely, electrons and holes. At a given temperature under equilibrium conditions, the product of the electron and hole concentrations is a constant.

$$n_0 p_0 = n_i^2$$

where n_0 and p_0 are the equilibrium electron and hole concentrations and $n_i$is the intrinsic carrier concentration. The followings are the bimolecular and monomolecular rate equations for n-type and p-type semiconductors. Bimolecular rate equation is

$$R = -\frac{dn}{dt} = -\frac{dp}{dt} = Bnp$$

Monomolecular rate equations are

For p-type semiconductors,

$$\frac{d}{dt}\Delta n(t) = -\frac{\Delta n(t)}{\tau_n}$$

For n-type semiconductors,

$$\frac{d}{dt}\Delta p(t) = -\frac{\Delta p(t)}{\tau_p}$$

where B is the recombination coefficient. After a short optical excitation pulse, the carrier decay in semiconductors can be measured by the decay of the luminescence. The recombination rate for low and high excitation cases are defined as follows [4].

For low-level excitation,

$$R = -\frac{dn(t)}{dt} = \frac{\Delta n_0}{\tau} e^{-t/\tau}$$

For high-level excitation,

$$R = -\frac{dn(t)}{dt} = \frac{-B}{\left(Bt + \Delta n_0^{-1}\right)^2}$$

6. Non-radiative Recombination

In non-radiative recombination events, the energy released during the electron-hole recombination is converted to phonons. During non-radiative recombination, the electron energy is converted to vibrational energy of lattice atoms, i.e. phonons. Thus, the electron energy is converted to heat. For obvious reasons, non-radiative recombination events are unwanted in light-emitting devices. The most common cause for non-radiative recombination events are defects in the crystal structure. There are many defects in semiconductor material [5].

The diagram for non-radiative recombination is shown in Figure 3.6. The first portion of the band diagram of non-radiative recombination is via deep level. The transition is between the energy gap. The recombination of free carriers via deep levels was first analyzed by Shockley, Read and Hall.

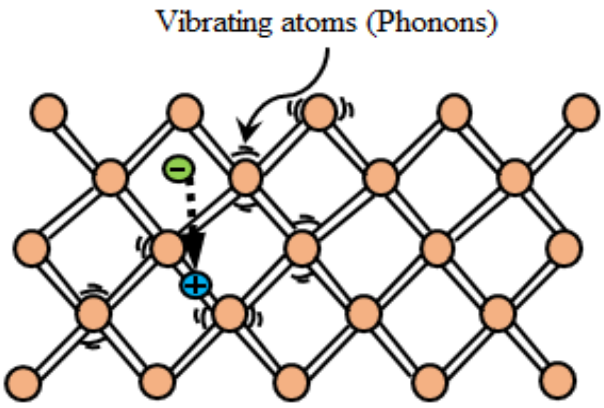

Figure 5 Non-Radiative Recombination Process [5]

$$R_{SR} = \frac{p_0 \Delta n + n_0 \Delta p + \Delta n \Delta p}{(N_T v_p \sigma_p)^{-1}(n_0 + n_1 + \Delta n) + (N_T v_n \sigma_n)^{-1}(p_0 + p_1 + \Delta p)}$$

where $\Delta n=\Delta p$; v_n and $v_p$are the electron and hole thermal velocities and σ_n and σ_p are the capture cross sections of the traps.

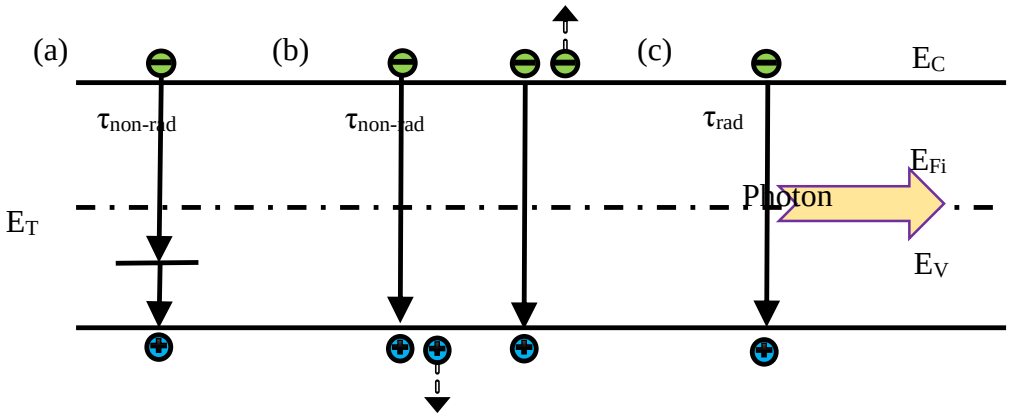

Figure 6 Band Diagram of Non-Radiative Recombination (a) via a Deep Level (b) via an Auger Recombination and (c) Radiative Recombination[5]

The second portion of another important non-radiative recombination mechanism is Auger recombination. Auger recombination is a three carrier process which may be band-to-band. In auger recombination, the energy is given to a third carrier, which is excited to a higher energy level without moving to another energy band. Auger effects mean that a second electron absorbs the energy given up by the first electron. In this process, the energy becoming available through electron-hole recombination is dissipated by the excitation of a free electron high into the conduction band, or by a hole deeply excited into the valence band. Auger recombination is proportional to the square of the carrier concentration since two carriers of the same type are required for the recombination process [5]. The last portion is radiative recombination. When electron and hole recombine with each other, light is emitted in the form of photons.

7. Surface Recombination

Non-radiative recombination can also occur at semiconductor surfaces. Surface recombination is the another important type of non-radiative recombination. Surface recombination occurs, when the optical laser excitation pulse at the surface, they absorb the energy.

Table 1The Surface Recombination Velocity for Some Semiconductors [6]

Semiconductor	Surface recombination velocity
GaAs	$S = 10^6$ cm/s
InP	$S = 10^3$ cm/s
Si	$S = 10^1$ cm/s
GaN	$S = 5x10^4$ cm/s

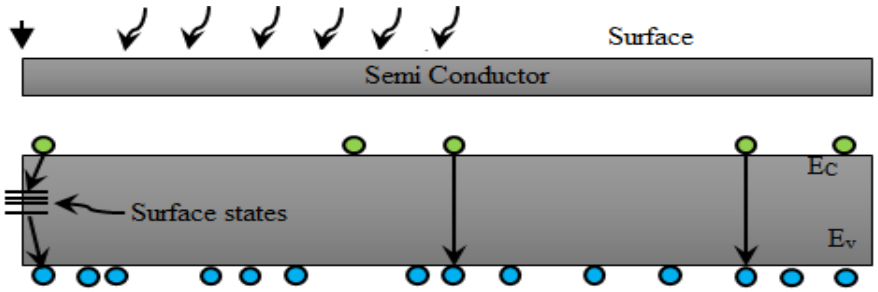

Figure 7 Illuminated p-type semiconductor and band diagram [6]

The transition process between bands occur, at each level of the surface states. Surface recombination leads to a reduced luminescence efficiency and also to heating of the surface due to non-radiative recombination at the surface. Both effects are unwanted in electroluminescent devices. So, surface recombination is not beneficial for light emitting diodes. The surface recombination velocities for some semiconductors are summarized in the following table [6].

8. Carrier Distribution in p-n Junction

A p-n junction with a donor concentration of N_D and an acceptor concentration of N_A has the free electron concentration of $n=N_D$ and the free hole concentration of $p=N_A$. It is further assumed that no compensation of the dopants occurs by unintentional impurities and defects. During an unbiased p-n junction, electrons originating from donors on the n-type side diffuse over to the p-type side where they encounter many holes with which they recombine. A corresponding process occurs with holes that diffuse to the n-type side. As a result, a region near the p-n junction is depleted of free carriers. This region is known as the depletion region.In the absence of free carriers in the depletion region, the only charge in the depletion region is from ionized donors and acceptors. These dopants form a space charge region, i.e. donors on the n-type side and acceptors on the p-type side. The space charge region produces a potential that is called the diffusion voltage V_D. The diffusion voltage is given by

$$V_D = \frac{kT}{e} \ln \frac{N_A N_D}{n_i^2}$$

where N_A and N_D is the acceptor and donor concentration. n_i is the intrinsic carrier concentration of the semiconductor [7].

The diffusion voltage represents the barrier that free carriers must overcome in order to reach the neutral region of opposite conductivity type. The width of the depletion region, the charge in the depletion region and the diffusion voltage are related by the Poisson equation [8].

The depletion layer width is

$$W_D = \sqrt{\frac{2\varepsilon}{e}(V - V_D)\left(\frac{1}{N_A} + \frac{1}{N_D}\right)}$$

where $\varepsilon = \varepsilon_r \varepsilon_0$, is the dielectric permittivity of the semiconductor and V is the diode bias voltage. Upon application of the bias voltage to the p-n junction, the voltage is going to drop across the depletion region. This region is highly resistive due to the fact that it is depleted of free carriers. An external bias therefore decreases or increases the p-n junction barrier for forward or reverse bias. Under forward bias conditions, electrons and holes are injected into the region with opposite conductivity type and current flow increases. The carriers diffuse into the regions of opposite conductivity type where they will eventually recombine, thereby emitting a photon [9].

9. Carrier Distribution in p-n Homojunctions

The carrier distribution in p-n homojunctions means that the p-n junctions consisting of a single material. In homojunction, the carriers diffuse over the diffusion length, before recombination. The large recombination region in homojunctions is not beneficial for efficient recombination. The mean distance a minority carrier diffuses before recombination is defined by the diffusion length.

$$L_n = \sqrt{D_n \tau_n} \qquad \text{and} \qquad L_p = \sqrt{D_p \tau_p}$$

where τ_n and τ_p are the electron and hole minority carrier lifetimes [10].

Also, the carrier distribution in p-n homojunctions depends on the diffusion constant of the carriers. The diffusion constant of carriers is not easily measured. The diffusion constant can be inferred from the carrier mobility by the Einstein relation for non-degenerate semiconductors is given by

$$D_n = \frac{kT}{e}\mu_n \qquad \text{and} \qquad D_p = \frac{kT}{e}\mu_p$$

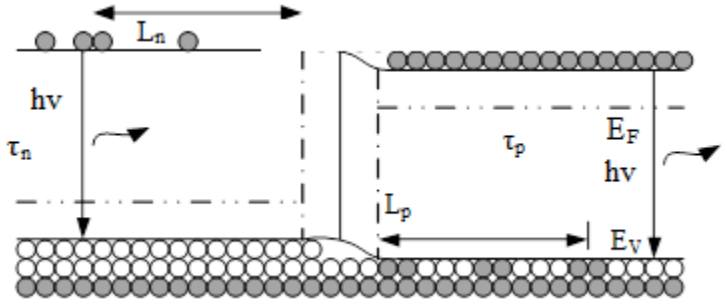

Figure 8 Homojunction Under Forward Bias [9]

10. Carrier Distribution in p-n Heterojunctions

Heterostructures confine free carriers to the small well region. They are frequently employed to obtain high carrier concentrations and thus short carrier lifetimes. All high intensity light emitting diodes do not use the homojunction design but rather employ heterojunctions, which have clear advantages over homojunction devices.

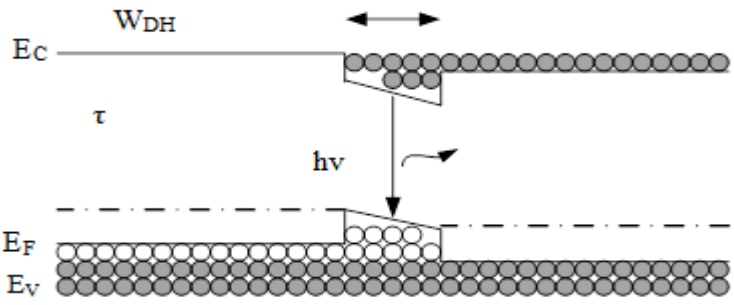

Figure 9 Heterojunction Under Forward Bias [11]

Heterojunction devices employ two types of semiconductors, namely a small-bandgap active region and a large-bandgap barrier region. In heterojunctions, carriers are confined to the well region. Bimolecular recombination equation is

$$R = Bnp$$

B is the recombination coefficient [11].

11. Double Heterostructure

If a structure consists of two barriers, i.e. two large-bandgap semiconductors, then the structure is called a double heterostructure. Double heterostructures are used for quantum well active regions. Today, all high efficiency LEDs use double heterostructure designs. A double heterostructure consists of a quantum well active region and two confinement layers. The confinement layers are frequently called cladding layers. A double heterostructure (DH) consists of the active region in which recombinations occur and two confinement layers cladding the active region. The two cladding or confinement layers have a larger band-gap than the active region [12]. There are two types of double heterostructure, namely, graded design and ungraded design. If the bandgap difference between the active and the confinement regions is ΔE_g then the band discontinuities occurring in the conduction and valence band follow the relation.

$$E_g\big|_{cladding} - E_g\big|_{active} = \Delta E_g = \Delta E_C + \Delta E_V$$

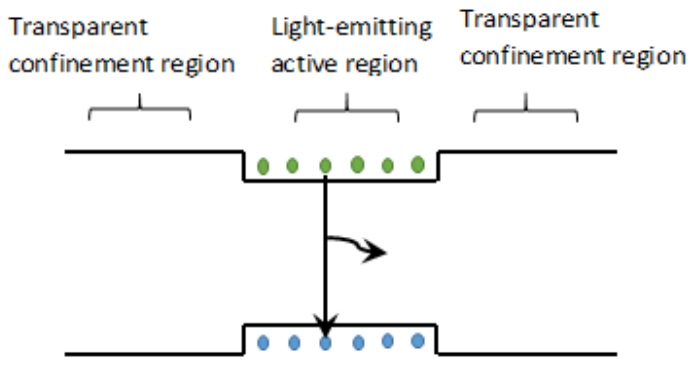

Figure 10 Double Heterostructure with Optically Transparent Confinement Regions [12]

12. Electron Blocking Layers

Carrier-blocking layers are used when carriers tend to escape from the active layer of an LED into the confinement layers. To reduce carrier leakage out of the active region, electron-blocking layers or electron blockers are used in many LED structures to reduce electron escape out of the active region.

Such electron blockers are regions with a high bandgap energy located at the confinement-active interface. The band diagram of a GaInN LED with an electron-blocking layer has been demonstrated.

The LED has AlGaN confinement layers and a GaInN/GaN multiple quantum well active regions. An AlGaN electron-blocking layer is included in the p-type confinement layer at the confinement-active interface.

In Figure.12 (a), showing the undoped structure, AlGaN electron-blocking layer creates a barrier to current flow in both the conduction band as well as the valence band. However in Figure.12 (b), showing the doped structure, there is no barrier to the flow of holes in the p-type confinement layer [13].

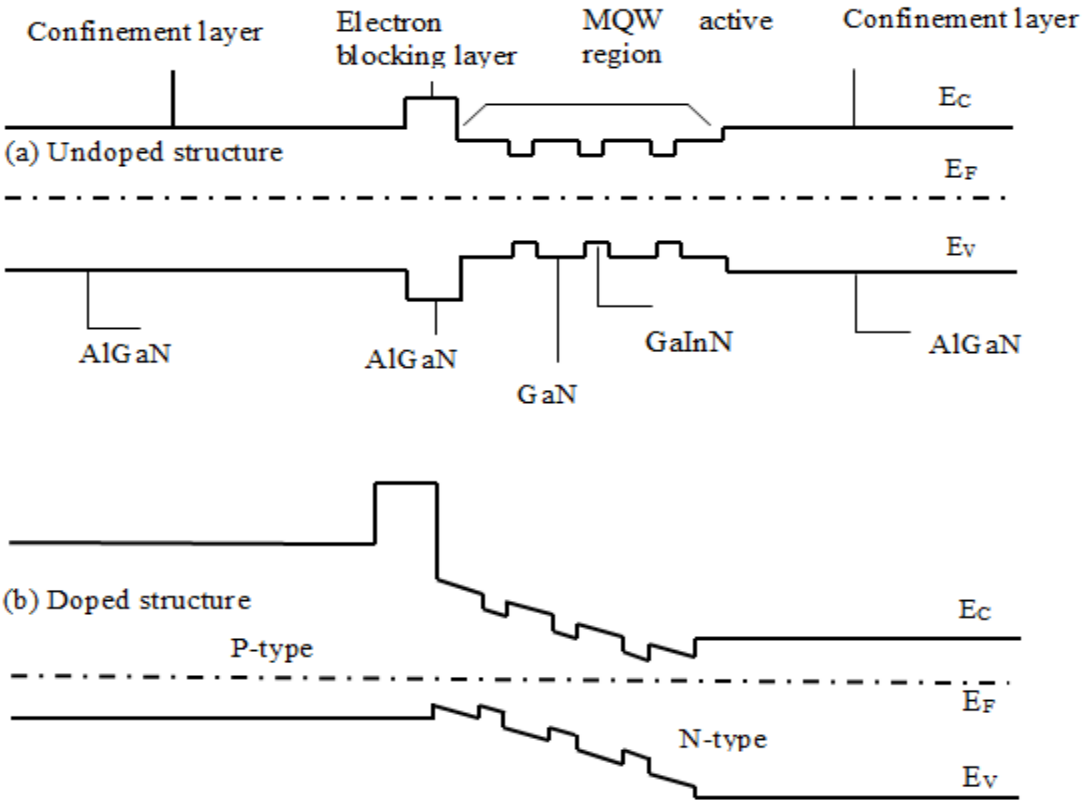

Figure 11 Illustration of an AlGaN Current-Blocking Layer in an AlGaN/GaN/ GaInN Multiquantum Well LED Structure. (a) Band Diagram without Doping (b) Band Diagram with Doping [13]

13. Current Equation

The Shockley equation for a diode with cross sectional area A is

$$I = eA\left\langle \sqrt{\frac{D_p}{\tau_p}}\frac{n_i^2}{N_D} + \sqrt{\frac{D_n}{\tau_n}}\frac{n_i^2}{N_A} \right\rangle \left(e^{eV/kT} - 1\right)$$

where $D_{n,p}$ and $\tau_{n,p}$ are the electron and hole diffusion constants and the electron and hole minority carrier lifetimes.

Under reverse bias conditions, the diode current saturates and the saturation current is given by the factor preceding the exponential function in the Shockley equation. The basic equation from the theory of semiconductors that mathematically describes the I-V characteristic of the light-emitting diode is

$$I = I_s\left(e^{eV/kT} - 1\right)$$

$$k = 1.38 \times 10^{-23}\ \text{J/K}$$

$$T = 300\text{K}$$

$$e = 1.6 \times 10^{-19}\ \text{C}$$

I_s is the saturation current.

$$I_s = eA\left[\sqrt{\frac{D_p}{\tau_p}}\frac{n_i^2}{N_D} + \sqrt{\frac{D_n}{\tau_n}}\frac{n_i^2}{N_A}\right]$$

A= cross-sectional area	D_p= hole diffusion constant
D_n = electron diffusion constant	n_i = intrinsic carrier concentration
τ_p= hole minority carrier lifetime	τ_n = electron minority carrier lifetime
τ_p= hole minority carrier lifetime	τ_n = electron minority carrier lifetime
N_D = donor concentration	N_A = acceptor concentration
k = Boltzmann's constant	T=room temperature
e=elementary charge	

Under typical forward bias conditions, the diode voltage is V>>kT/e, and thus $[\exp(eV/kT) - 1] \approx \exp(eV/kT)$.

$$I = eA\left\langle \sqrt{\frac{D_p}{\tau_p}}N_A + \sqrt{\frac{D_n}{\tau_n}}N_D \right\rangle \left(e^{e(V - V_D)/kT}\right)$$

The current strongly increases as the diode voltage approaches the diffusion voltage, i.e. $V \sim V_D$. The voltage at which the current strongly increases is called the threshold voltage and this voltage is given by $V_{th}=V_D$. Several diode I-V characteristics of semiconductors made from different materials are along with the bandgap energy of the materials. The comparison with the bandgap

energy of different materials indicates that the energy gap and the threshold voltage indeed agree reasonably well.

14. Temperature Dependence of Band-Gap Energy

As the temperature increases, the energy gap of semiconductors decreases. The temperature dependence of the energy gap of a semiconductor can be expressed by the formula called the Varshni Formula (Varshni, 1967).

$$E_g = E_g(0K) - \frac{\alpha T^2}{T + \beta}$$

where E_g = band-gap energy, T = temperature (K), α and β = fitting parameters

The fitting parameters are frequently called the Varshni parameters. The Varshni parameters of common semiconductors are summarized in the table. The bandgap energy versus temperature for several semiconductors is along with the values for α and β. Assuming that the change in band-gap energy is the dominant factor in determining the temperature dependence of the diode voltage, the temperature dependence of the forward voltage follows directly from the temperature.

Table 2 The Varshni Parameters of Semiconductors

	E_g(0K)	**α (10^{-4} eV/K)**	**β (K)**
GaN	3.470	7.70	600
GaP	2.340	6.20	460
GaAs	1.519	5.41	204
InP	1.425	4.50	327
Si	1.170	4.73	636
Ge	0.744	4.77	235
AlN	6.026	18.0	1462
GaSb	0.813	3.78	94
InN	1.994	2.45	624
InAs	0.415	2.76	83

15. The Temperature Dependence of Emission Intensity

The temperature dependence of emission intensity is defined by the following equation.

$$I = I_{0K} \exp(-T/T_1)$$

where T_1 is the characteristic temperature that describes the temperature dependence of the LED. A high characteristic temperature is desirable, which implies a small temperature dependence. It is interesting to note that both LEDs as well as semiconductor lasers have a distinct temperature dependence of the emission intensity. In LEDs, the decrease is expressed in terms of "T_1 equation". The characteristic temperature with the associate wavelength and colors of LEDs are summarized in the following table. The emission intensity of LEDs decreases with increasing temperature.

This decrease of the emission intensity is due to several temperature-dependent factors including (i) non-radiative recombination via deep levels, (ii) surface recombination, and (iii) carrier loss over heterostructure barriers. The characteristic temperature with wavelength is described in the following.

Table 3 The Characteristic Temperature with the Associate Wavelength and Colors

GaInN/GaN Green LEDs	525nm	T_1 = 295K
GaInN/GaN Blue LEDs	470nm	T_1 = 1600K
AlGaInP/GaAs Red LEDs	625nm	T_1 = 95K
GaInN Cyan LEDs	505nm	T_1 = 832K
AlGaInP Red LEDs	625nm	T_1 = 199K
GaInN Green LEDs	527nm	T_1 = 341K

16. Band Diagram of a p-GaAs/N-$Al_{0.3}Ga_{0.7}As$ Heterojunction

The energy band structure for p-GaAs/N-$Al_{0.3}Ga_{0.7}As$ heterojunction is analysed by using the appropriate parameters. The mole fraction (x) is 0.3. By analyzing the energy band structure, the effect of the forward voltage or barrier voltage can be observed, especially from the differences in energy gap. For p-GaAs/N-$Al_xGa_{1-x}As$ (x=0.3), acceptor concentration for p side is

$$N_a = 1 \times 10^{18}\ cm^{-3}$$

Donor concentration for N side is

$$N_D = 2 \times 10^{17}\ cm^{-3}$$

Assume that the density of states hole effective mass ($0 \le x \le 0.45$) is

$$m_h^*(x) = (0.50 + 0.29x)m_0$$

Electron effective mass is

$$m_e^*(x) = (0.0665 + 0.083x)m_0$$

The energy gap is

$$E_g(x) = (1.424 + 1.247x)(eV)$$

Dielectric constant for ($0 \le x \le 0.45$),

$$\varepsilon(x) = (13.1 - 3x)\varepsilon_0$$

x is the mole fraction of aluminium.

$\varepsilon_0 = 8.854 \times 10^{-14}$ As/ (Vcm)

$k_B = 8.6175 \times 10^{-5}$ eV/K

For x=0.3,

The band edge discontinuities are

$\Delta E_g = 1.247x$

$\Delta E_c = 0.67 \Delta E_g$

$\Delta E_v = 0.33 \Delta E_g$

Table.4.

Table 4 Band Structure Parameters for p-GaAs/N-AlGaAs

p-GaAs	N-$Al_xGa_{1-x}As$
$m_e^* = 0.0665m_0$	$m_e^* = 0.0914m_0$
$m_h^* = 0.50m_0$	$m_h^* = 0.587m_0$
$\varepsilon_p = 13.1 \varepsilon_0$	$\varepsilon_N = 12.2 \varepsilon_0$
$E_{gp} = 1.424$eV	$E_{gN} = 1.798$eV

The concentrations are

$$N_c = 2.51 \times 10^{19} \left[\frac{m_e^*}{m_0} \frac{T}{300} \right]^{3/2} \text{cm}^{-3}$$

$$N_v = 2.51 \times 10^{19} \left[\frac{m_h^*}{m_0} \frac{T}{300} \right]^{3/2} \text{cm}^{-3}$$

$$p = N_a = N_v F_{1/2} \left[\frac{E_{vp} - F_p}{k_B T} \right] = N_v \exp \left[\frac{E_{vp} - F_p}{k_B T} \right]$$

$$F_p - E_{vp} = -k_B T \ln \frac{N_a}{N_v}$$

$$N = N_D = N_c F_{1/2} \left[\frac{F_N - E_{cN}}{k_B T} \right] = N_c \exp \left[\frac{F_N - E_{cN}}{k_B T} \right]$$

$$E_{cN} - F_N = -k_B T \ln \frac{N_D}{N_c}$$

$$V_0 = \frac{E_{gp} + \Delta E_c - \left(F_p - E_{vp}\right) - \left(E_{cN} - F_N\right)}{q}$$

The depletion widths are as follows.

$$x_p = \left[\frac{2\varepsilon_p V_0}{qN_a N_D \left(N_D + \frac{\varepsilon_p}{\varepsilon_N} N_a \right)} \right]^{1/2} N_D$$

$$x_N = \frac{x_p}{N_D} N_a$$

$$x_w = x_p + x_N$$

The voltage drop across p-side is

$$V_{op} - V_p = \frac{qN_a}{2\varepsilon_p} x_p^2$$

Also, the voltage drop across N-side is

$$V_{oN} - V_N = \frac{qN_D}{2\varepsilon_N} x_N^2$$

17. Band Diagram of n-GaAs/P-$Al_{0.3}Ga_{0.7}As$ Heterojunction

The energy band structure for n-GaAs/P-$Al_{0.3}Ga_{0.7}As$ heterojunction is analysed by using the appropriate parameters. The mole fraction (x) is 0.3. For the energy band design, the step by step procedure to find the band structure is similar to that of the homojunction except that there are no band edge discontinuities in homojunction.

For n-GaAs/P-$Al_{0.3}Ga_{0.7}As$, the parameter usages are as follows.

Acceptor concentration for n region is

$$N_d = 4 \times 10^{16} \text{ cm}^{-3}$$

Donor concentration for P region is

$$N_A = 2 \times 10^{17}\ cm^{-3}$$

Assume that the density of states hole effective mass ($0 \leq x \leq 0.45$) is

$$m_h^*(x) = (0.50 + 0.29x)m_0$$

Electron effective mass is

$$m_e^*(x) = (0.0665 + 0.083x)m_0$$

The energy gap is

$$E_g(x) = (1.424 + 1.247x)(eV)$$

Dielectric constant for ($0 \leq x \leq 0.45$),

$$\varepsilon(x) = (13.1 - 3x)\varepsilon_0$$

x is the mole fraction of aluminium.

$$\varepsilon_0 = 8.854 \times 10^{-14}\ As/(Vcm)$$

$$k_B = 8.6175 \times 10^{-5}\ eV/K$$

The band edge discontinuities are

$$\Delta E_g = 1.247x$$

$$\Delta E_c = 0.67\ \Delta E_g$$

$$\Delta E_v = 0.33\ \Delta E_g$$

Table 5 Band Structure Parameters for n-GaAs/P-AlGaAs

n-GaAs	P-$Al_{0.3}Ga_{0.7}As$
$m_e^* = 0.0665m_0$	$m_e^* = 0.0914m_0$
$m_h^* = 0.50m_0$	$m_h^* = 0.587m_0$
$\varepsilon_n = 13.1\ \varepsilon_0$	$\varepsilon_P = 12.2\ \varepsilon_0$
$E_{gn} = 1.424eV$	$E_{GP} = 1.798eV$

$$N_c = 2.51 \times 10^{19} \left[\frac{m_e^*}{m_0} \frac{T}{300} \right]^{3/2} \quad cm^{-3}$$

$$N_v = 2.51 \times 10^{19} \left[\frac{m_h^*}{m_0} \frac{T}{300} \right]^{3/2} \quad cm^{-3}$$

$$n = N_d = N_c F_{1/2} \left[\frac{F_n - E_{cn}}{k_B T} \right] = N_c \exp \left[\frac{F_n - E_{cn}}{k_B T} \right]$$

$$E_{cn} - F_n = -k_B T \ln \frac{N_d}{N_c}$$

$$P = N_A = N_v F_{1/2} \left[\frac{E_{vP} - F_P}{k_B T} \right] = N_v \exp \left[\frac{E_{vP} - F_P}{k_B T} \right]$$

$$F_P - E_{vP} = -k_B T \ln \frac{N_A}{N_v}$$

The contact potential is as follows.

$$V_0 = \frac{E_{GP} - \Delta E_c - (E_{cn} - F_n) - (F_P - E_{vP})}{q}$$

The depletion widths

$$x_n = \left[\frac{2 \varepsilon_n V_0}{q N_d N_A \left(N_A + \frac{\varepsilon_n}{\varepsilon_P} N_d \right)} \right]^{1/2} N_A$$

$$x_P = \frac{x_n}{N_A} N_d$$

$$x_w = x_n + x_P$$

The voltage drop across the n-side

$$V_{on} - V_n = \frac{qN_d}{2\varepsilon_n} x_n^2$$

The voltage drop across the P-side

$$V_{oP} - V_P = \frac{qN_A}{2\varepsilon_P} x_P^2$$

18. Band Diagram of an Unbiased n-InN/P-GaN Heterojunction

The energy band structure for n-InN/P-GaN heterojunction is analysed by using the appropriate parameters. The step by step procedure to find the n-P band structure is similar to that of the p-N design.

For n-InN/P-GaN (heterostructure), the parameter usages are as follows.

Table 6 Band Structure Parameters for n-InN/P-GaN

n-InN	P-GaN
$m_e^* = 0.11m_0$	$m_e^* = 0.20m_0$
$m_h^* = 0.27m_0$	$m_h^* = 0.8m_0$
$\varepsilon_n = 15.3\ \varepsilon_0$	$\varepsilon_P = 8.9\ \varepsilon_0$
$E_{gn} = 0.77eV$	$E_{GP} = 3.4eV$

Donor concentration is $N_d = 4.7 \times 10^{18} cm^{-3}$ (n region)

Acceptor concentration is $N_A = 1 \times 10^{18} cm^{-3}$ (P region)

Dielectric constant is $\varepsilon_0 = 8.854 \times 10^{-14} As/(Vcm)$

Boltzmann's constant $k_B = 8.6175 \times 10^{-5} eV/K$

19. Band Diagram of a p-ZnCdO/N-ZnCdO Homojunction

The energy band structure for p-ZnCdO/N-ZnCdO homojunction is analysed by using the appropriate parameters. The step by step procedure to find the band structure is similar to that of the homojunction except that there are no band edge discontinuities in homojunction.

For ZnCdO (homostructure), the parameter usages are as follows.

$N_a = 1 \times 10^{17} cm^{-3}$ (p side)

$N_D = 1 \times 10^{18} cm^{-3}$ (N side)

$\varepsilon_0 = 8.854 \times 10^{-14} As/(Vcm)$

$$N_c = 2.51 \times 10^{19} \left[\frac{m_e^*}{m_0} \frac{T}{300} \right]^{3/2} \quad cm^{-3}$$

Table 7 Band Structure Parameters for p-ZnCdO/N-ZnCdO

p-ZnCdO	N-ZnCdO
$m_e^* = 0.24 m_0$	$m_e^* = 0.24 m_0$
$m_h^* = 0.6 m_0$	$m_h^* = 0.6 m_0$
$\varepsilon_p = 8.45 \varepsilon_0$	$\varepsilon_N = 8.45 \varepsilon_0$
$E_{gp} = 3.1eV$	$E_{gN} = 3.1eV$

$$N_v = 2.51 \times 10^{19} \left[\frac{m_h^*}{m_0} \frac{T}{300} \right]^{3/2} \quad cm^{-3}$$

$$p = N_a = N_v F_{1/2} \left[\frac{E_{vp} - F_p}{k_B T} \right] = N_v \exp \left[\frac{E_{vp} - F_p}{k_B T} \right]$$

$$F_p - E_{vp} = -k_B T \ln \frac{N_a}{N_v}$$

$$N = N_D = N_c F_{1/2} \left[\frac{F_N - E_{cN}}{k_B T} \right] = N_c \exp \left[\frac{F_N - E_{cN}}{k_B T} \right]$$

$$E_{cN} - F_N = -k_B T \ln \frac{N_D}{N_c}$$

The contact potential

$$V_0 = \frac{E_{gp} - (F_p - E_{vp}) - (E_{cN} - F_N)}{q}$$

The depletion widths

$$x_p = \left[\frac{2 \varepsilon_p V_0}{q N_a N_D \left(N_D + \frac{\varepsilon_p}{\varepsilon_N} N_a \right)} \right]^{1/2} N_D$$

$$x_N = \frac{x_p}{N_D} N_a$$

$$x_w = x_p + x_N$$

20. Band Diagram of an Unbiased n-ZnO/P-$Al_{0.16}Ga_{0.84}N$ Heterojunction

The band structure for n-ZnO/P-$Al_{0.16}Ga_{0.84}N$ heterojunction is analysed by using the appropriate parameters. The mole fraction of the material (x) is 0.16. For n-ZnO/P-$Al_{0.16}Ga_{0.84}N$, the parameter usages are as follows.

Table 8 Band structure parameters for n-ZnO/P-AlGaN

n-ZnO	P-AlGaN
$m_e^* = 0.28m_0$	$m_e^* = 0.36m_0$
$m_h^* = 0.59m_0$	$m_h^* = 0.8m_0$
$\varepsilon_n = 8.5\ \varepsilon_0$	$\varepsilon_P = 8.9\ \varepsilon_0$
$E_{gn} = 3.37eV$	$E_{GP} = 3.4eV$

The doping concentrations for the heterojunction are in the following.

$N_d = 1 \times 10^{17}\ cm^{-3}$ (n region)

$N_A = 2 \times 10^{16}\ cm^{-3}$ (P region)

$\varepsilon_0 = 8.854 \times 10^{-14}\ As/(Vcm)$

$k_B = 8.6175 \times 10^{-5}\ eV/K$

21. Band Diagram of a p-Si/N-Si Homojunction

The energy band structure for p-Si/N-Si homojunction is analysed by using the appropriate parameters.

For silicon (homostructure), the parameter usages are as follows.

Table 9 Band Structure Parameters for p-Si/N-Si

p-Si	N-Si
$m_e^* = 0.98m_0$	$m_e^* = 0.98m_0$
$m_h^* = 0.49m_0$	$m_h^* = 0.49m_0$
$\varepsilon_p = 11.7\ \varepsilon_0$	$\varepsilon_N = 11.7\ \varepsilon_0$
$E_{gp} = 1.12eV$	$E_{gN} = 1.12eV$

$N_a = 3 \times 10^{15}\ cm^{-3}$ (p side)

$N_D = 1 \times 10^{16}\ cm^{-3}$ (N side)

$\varepsilon_0 = 8.854 \times 10^{-14}\ As/(Vcm)$

$k_B = 8.6175 \times 10^{-5}\ eV/K$

22. Band Diagram of a p-Ge/N-Ge Homojunction

The energy band structure for p-Si/N-Si homojunction is analysed by using the appropriate parameters.

For germanium (homostructure), the parameter usages are as follows.

$N_a = 1 \times 10^{16}\ cm^{-3}$ (p side)

$N_D = 5 \times 10^{13}\ cm^{-3}$ (N side)

$\varepsilon_0 = 8.854 \times 10^{-14}\ As/(Vcm)$

Table 10 Band Structure Parameters for p-Ge/N-Ge

p-Ge	N-Ge
$m_e^* = 1.6m_0$	$m_e^* = 1.6m_0$
$m_h^* = 0.28m_0$	$m_h^* = 0.28m_0$
$\varepsilon_p = 16.2\ \varepsilon_0$	$\varepsilon_N = 16.2\ \varepsilon_0$
$E_{gp} = 0.66eV$	$E_{gN} = 0.66eV$

23. Band Diagram of a p-$CsPbBr_3$/N- $CsPbBr_3$ Homojunction

The energy band structure for p-$CsPbBr_3$/N-$CsPbBr_3$ homojunction is analysed by using the appropriate parameters. From the design of the band diagram, the conditions of the drift current or diffusion current flowing across the homojunction can be observed.

For $CsPbBr_3$ homostructure, the parameter usages are as follows.

Table 11 Band Structure Parameters for p-CsPbBr3/N-CsPbBr3

p-$CsPbBr_3$	N-$CsPbBr_3$
$m_e^* = 0.15m_0$	$m_e^* = 0.15m_0$
$m_h^* = 0.14m_0$	$m_h^* = 0.14m_0$
$\varepsilon_p = 5\varepsilon_0$	$\varepsilon_N = 5\varepsilon_0$
$E_{gp} = 2.25eV$	$E_{gN} = 2.25eV$

For $CsPbBr_3$ (homostructure), p-$CsPbBr_3$ /N-$CsPbBr_3$,

$N_a = 2 \times 10^{18}\ cm^{-3}$ (p side)

$N_D = 5 \times 10^{17}\ cm^{-3}$ (N side)

$\varepsilon_0 = 8.854 \times 10^{-14}\ As/(Vcm)$

24. Current-Voltage Characteristics of Materials

The proper V-I characteristics of some materials used for light emitting diodes are described. The material systems include the p-N and n-P for both homojunction and heterojunction structure. The required data for the materials such as concentration, diffusion constant, carrier lifetime are mentioned in this article. The associate current-voltage characteristics curves are shown with figures in the following. For p-GaAs/N-$Al_{0.3}Ga_{0.7}As$, the current equation is

$$I = I_s\left(e^{eV/kT} - 1\right)$$

Cross-sectional area, $A = 2 \times 10^{-4}\ cm^2$

Acceptor concentration, $N_A = 1 \times 10^{18}\ cm^{-3}$

Donor concentration, $N_D = 2 \times 10^{17}\ cm^{-3}$

Intrinsic carrier concentration for GaAs, $n_i = 2 \times 10^{6}\ cm^{-3}$

Intrinsic carrier concentration for AlGaAs, $n_i = 2.1 \times 10^{3}\ cm^{-3}$

Electron diffusion constant, $D_n = 57.5 cm^2/s$

Hole diffusion constant, $D_p = 10 cm^2/s$

Electron carrier lifetimes, $\tau_n = 19 \times 10^{-9}\ s$

Hole carrier lifetimes, $\tau_p = 1 \times 10^{-8}\ s$

The saturation current is

$$I_s = eA\left\langle \sqrt{\frac{D_p}{\tau_p}}\frac{n_i^2}{N_D} + \sqrt{\frac{D_n}{\tau_n}}\frac{n_i^2}{N_A} \right\rangle = 7.042 \times 10^{-24}\ A$$

The current equation is $I = I_s\left(e^{eV/kT} - 1\right)$

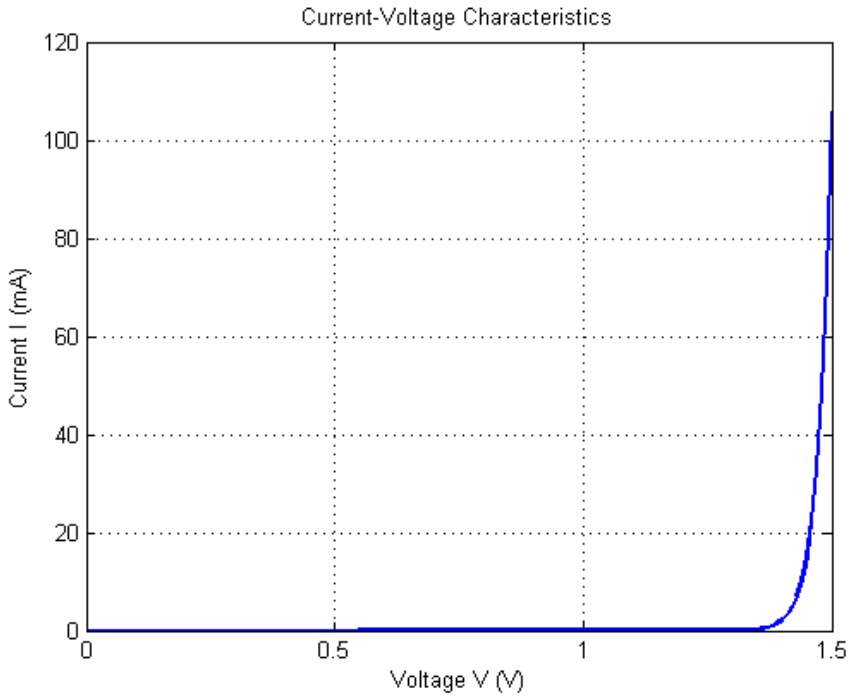

Figure 12 Current-Voltage Characteristics of p-GaAs/N-Al0.3Ga0.7As

For n-GaAs/P-$Al_{0.3}Ga_{0.7}As$, cross-sectional area, $A = 2 \times 10^{-4}\ cm^2$

Acceptor concentration, $N_A = 2 \times 10^{17}\ cm^{-3}$

Donor concentration, $N_D = 4 \times 10^{16}\ cm^{-3}$

Intrinsic carrier concentration for GaAs, $n_i = 2 \times 10^{6}\ cm^{-3}$

Intrinsic carrier concentration for AlGaAs, $n_i = 2.1 \times 10^{3}\ cm^{-3}$

Electron diffusion constant, $D_n = 57.5 cm^2/s$

Hole diffusion constant, $D_p = 10 cm^2/s$

Electron carrier lifetimes, $\tau_n = 19 \times 10^{-9} s$

Hole carrier lifetimes, $\tau_p = 1 \times 10^{-8} s$

The saturation current is $I_s = eA\left\langle \sqrt{\frac{D_p}{\tau_p}}\frac{n_i^2}{N_D} + \sqrt{\frac{D_n}{\tau_n}}\frac{n_i^2}{N_A} \right\rangle = 1.012 \times 10^{-22} A$

The current equation is

$$I = I_s\left(e^{eV/kT} - 1\right)$$

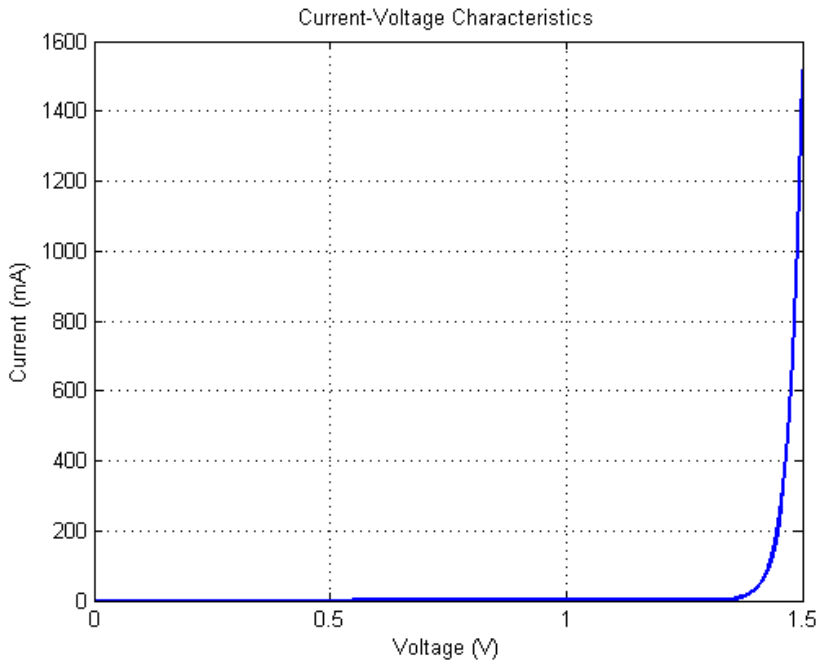

Figure 13 Current-Voltage Characteristics of n-GaAs/P-Al0.3Ga0.7As

For n-InN/P-GaN, the current equation is

$$I = I_s\left(e^{eV/kT} - 1\right)$$

Cross-sectional area, $A = 2 \times 10^{-4}\,cm^2$

Acceptor concentration, $N_A = 1 \times 10^{18}\,cm^{-3}$

Donor concentration, $N_D = 4.7 \times 10^{18}\,cm^{-3}$

Intrinsic carrier concentration for InN, $n_i = 920cm^{-3}$

Intrinsic carrier concentration for GaN, $n_i = 1.9 \times 10^{-10}\,cm^{-3}$

Electron diffusion constant, $D_n = 39cm^2/s$

Hole diffusion constant, $D_p = 0.75cm^2/s$

Electron carrier lifetimes, $\tau_n = 1 \times 10^{-8}\,s$

Hole carrier lifetimes, $\tau_p = 1 \times 10^{-8}\,s$

The saturation current is $I_s = eA\left\langle\sqrt{\frac{D_p}{\tau_p}}\frac{n_i^2}{N_D} + \sqrt{\frac{D_n}{\tau_n}}\frac{n_i^2}{N_A}\right\rangle = 4.99072 \times 10^{-32}\,A$

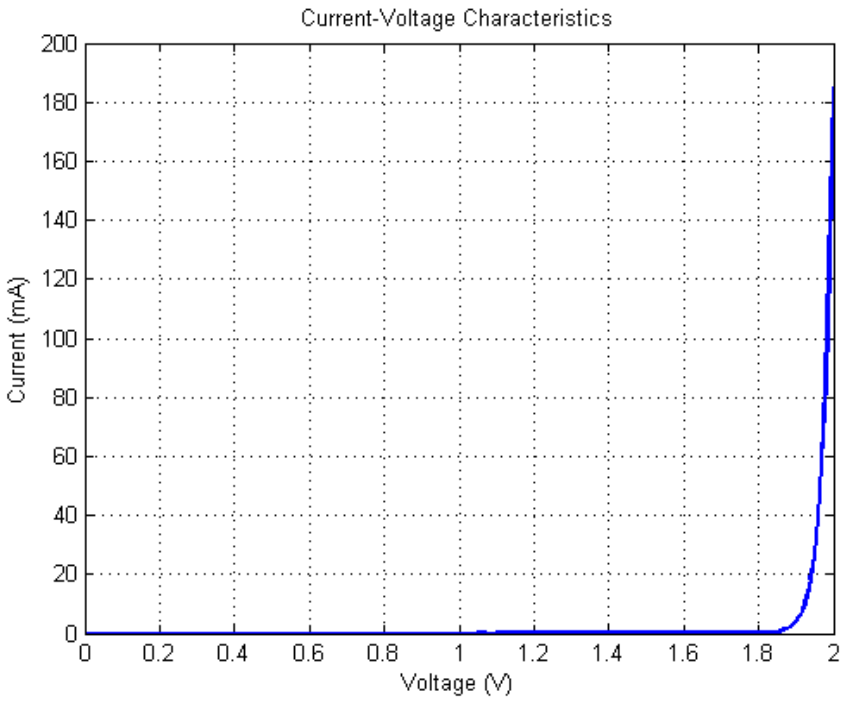

Figure 14 Current-Voltage Characteristics of n-InN/P-GaN

For ZnCdO, the current equation is $I = I_s\left(e^{eV/kT} - 1\right)$

The relative parameters are as follows.

Cross-sectional area, $A = 2 \times 10^{-4}\,\mathrm{cm}^2$

Acceptor concentration, $N_A = 1 \times 10^{17}\,\mathrm{cm}^{-3}$

Donor concentration, $N_D = 1 \times 10^{18}\,\mathrm{cm}^{-3}$

Intrinsic carrier concentration, $n_i = 1 \times 10^{15}\,\mathrm{cm}^{-3}$

Electron diffusion constant, $D_n = 0.01\mathrm{cm}^2/\mathrm{s}$

Hole diffusion constant, $D_p = 0.02\mathrm{cm}^2/\mathrm{s}$

Carrier lifetimes, $\tau_n = \tau_p = 2.1 \times 10^{-9}\,\mathrm{s}$

The saturation current is $I_s = eA\left\langle \sqrt{\frac{D_p}{\tau_p}}\frac{n_i^2}{N_D} + \sqrt{\frac{D_n}{\tau_n}}\frac{n_i^2}{N_A} \right\rangle$

$= 7.971 \times 10^{-7}\,\mathrm{A}$

The result figure is in the following.

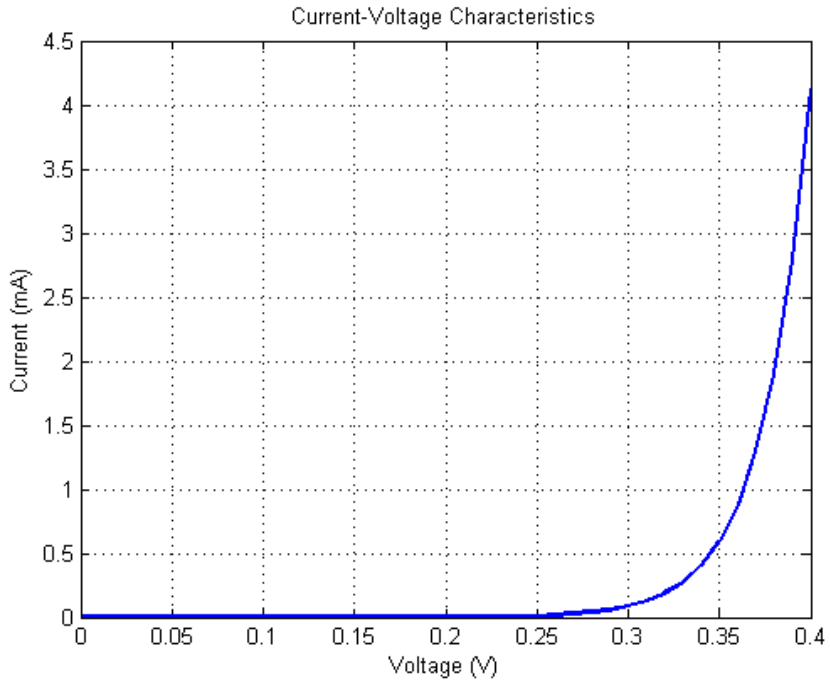

Figure 15 Current-Voltage Characteristics of ZnCdO

For n-ZnO/P-$Al_{0.16}Ga_{0.84}N$, the current equation is $I = I_s\left(e^{eV/kT} - 1\right)$

Cross-sectional area, $A = 2 \times 10^{-4}\,cm^2$

Acceptor concentration, $N_A = 2 \times 10^{16}\,cm^{-3}$

Donor concentration, $N_D = 1 \times 10^{17}\,cm^{-3}$

Intrinsic carrier concentration for ZnO, $n_i = 106 cm^{-3}$

Intrinsic carrier concentration for AlGaN, $n_i = 2.9 \times 10^{-9}\,cm^{-3}$

Electron diffusion constant, $D_n = 40 cm^2/s$

Hole diffusion constant, $D_p = 0.012 cm^2/s$

Electron carrier lifetimes, $\tau_n = 1 \times 10^{-8}\,s$

Hole carrier lifetimes, $\tau_p = 2 \times 10^{-9}\,s$

The saturation current is $I_s = eA\left\langle \sqrt{\frac{D_p}{\tau_p}}\frac{n_i^2}{N_D} + \sqrt{\frac{D_n}{\tau_n}}\frac{n_i^2}{N_A} \right\rangle = 8.81 \times 10^{-33}\,A$

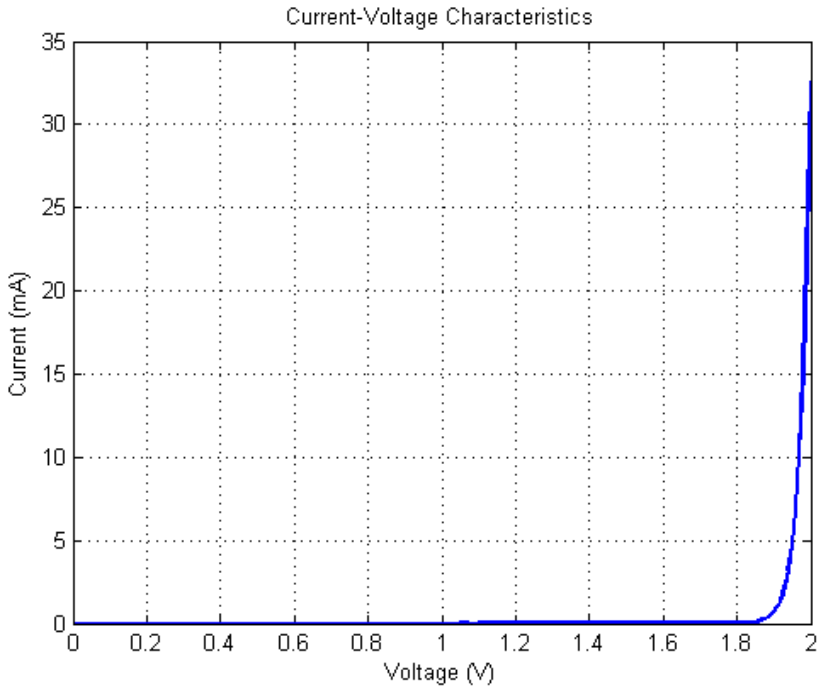

Figure 16 Current-Voltage Characteristics of n-ZnO/P-Al0.16Ga0.84N

For silicon, the current equation is

$$I = I_s\left(e^{eV/kT} - 1\right)$$

Cross-sectional area, $A = 2 \times 10^{-4}\,cm^2$
Acceptor concentration, $N_A = 3 \times 10^{15}\,cm^{-3}$
Donor concentration, $N_D = 10^{16}\,cm^{-3}$
Intrinsic carrier concentration, $n_i = 1 \times 10^{10}\,cm^{-3}$
Electron diffusion constant, $D_n = 39cm^2/s$
Hole diffusion constant, $D_p = 12cm^2/s$
Carrier lifetimes, $\tau_p = \tau_n = 1 \times 10^{-6}\,s$

The saturation current is

$$I_s = eA\left\langle\sqrt{\frac{D_p}{\tau_p}}\frac{n_i^2}{N_D} + \sqrt{\frac{D_n}{\tau_n}}\frac{n_i^2}{N_A}\right\rangle = 7.7698 \times 10^{-15}\,A$$

The result figure of the current-voltage characteristic is in the following.

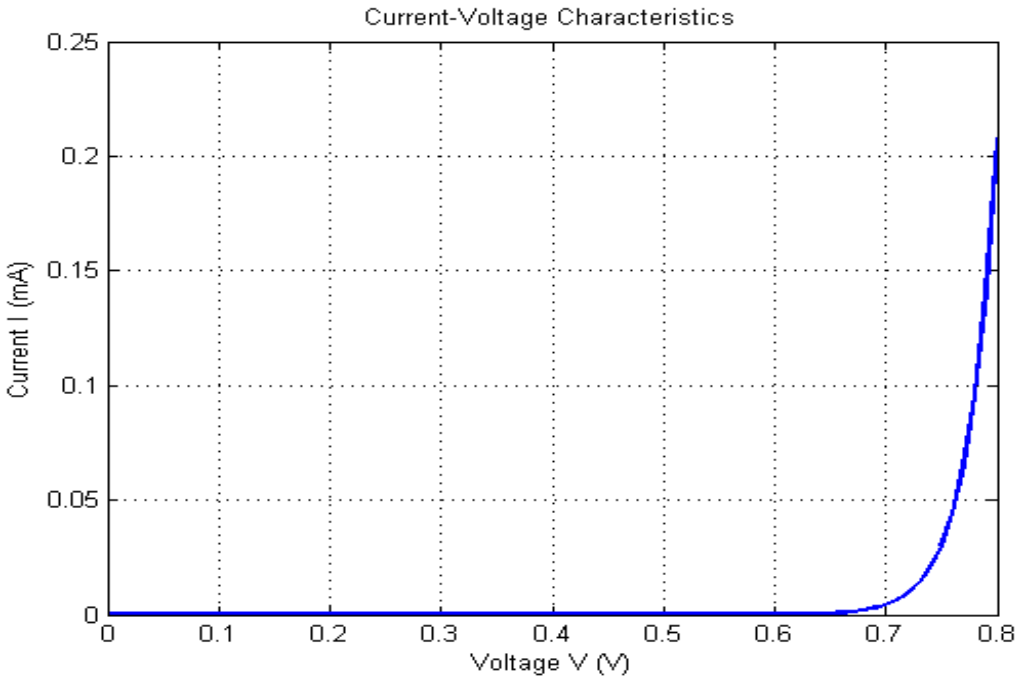

For germanium, the current equation is

$$I = I_s\left(e^{eV/kT} - 1\right)$$

Cross-sectional area, $A = 2 \times 10^{-4}\,cm^2$

Acceptor concentration, $N_A = 1 \times 10^{16}\,cm^{-3}$

Donor concentration, $N_D = 5 \times 10^{13}\,cm^{-3}$

Intrinsic carrier concentration, $n_i = 2 \times 10^{13}\,cm^{-3}$

Electron diffusion constant, $D_n = 101 cm^2/s$

Hole diffusion constant, $D_p = 49 cm^2/s$

Carrier lifetimes, $\tau_p = \tau_n = 1 \times 10^{-6} s$

The saturation current is $I_s = eA\left\langle \sqrt{\frac{D_p}{\tau_p}}\frac{n_i^2}{N_D} + \sqrt{\frac{D_n}{\tau_n}}\frac{n_i^2}{N_A} \right\rangle = 1.805 \times 10^{-6} A$

For germanium, the current-voltage characteristic curve is as shown in Figure.19. The forward voltage of the device is 0.3 V.

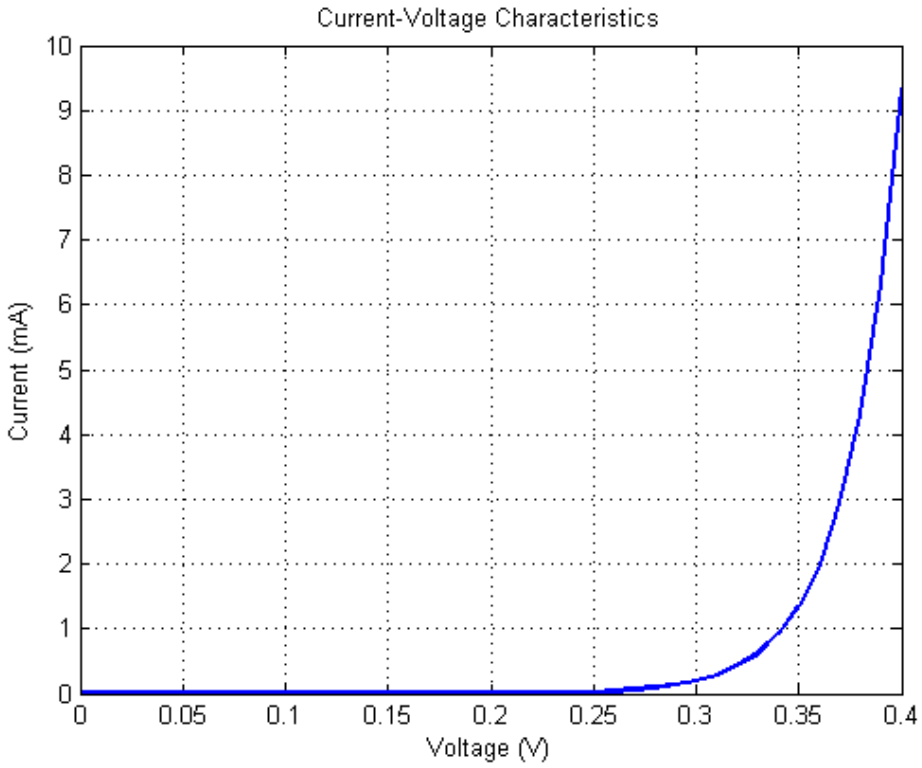

Figure 19 Current-Voltage Characteristic of Germanium

For $CsPbBr_3$, the current equation is

$$I = I_s\left(e^{eV/kT} - 1\right)$$

Cross-sectional area, $A = 2 \times 10^{-4}\,cm^2$
Acceptor concentration, $N_A = 2 \times 10^{18}\,cm^{-3}$
Donor concentration, $N_D = 5 \times 10^{17}\,cm^{-3}$
Intrinsic carrier concentration, $n_i = 201 cm^{-3}$
Electron diffusion constant, $D_n = 5 \times 10^{-6}\,cm^2/s$
Hole diffusion constant, $D_p = 3 \times 10^{-4}\,cm^2/s$
Carrier lifetimes, $\tau_n = \tau_p = 12.3 \times 10^{-9}\,s$

The saturation current is in the following.

$$I_s = eA\left\langle \sqrt{\frac{D_p}{\tau_p}}\frac{n_i^2}{N_D} + \sqrt{\frac{D_n}{\tau_n}}\frac{n_i^2}{N_A} \right\rangle = 4.17 \times 10^{-34}\,A$$

The associated current-voltage characteristic is in the following figure.

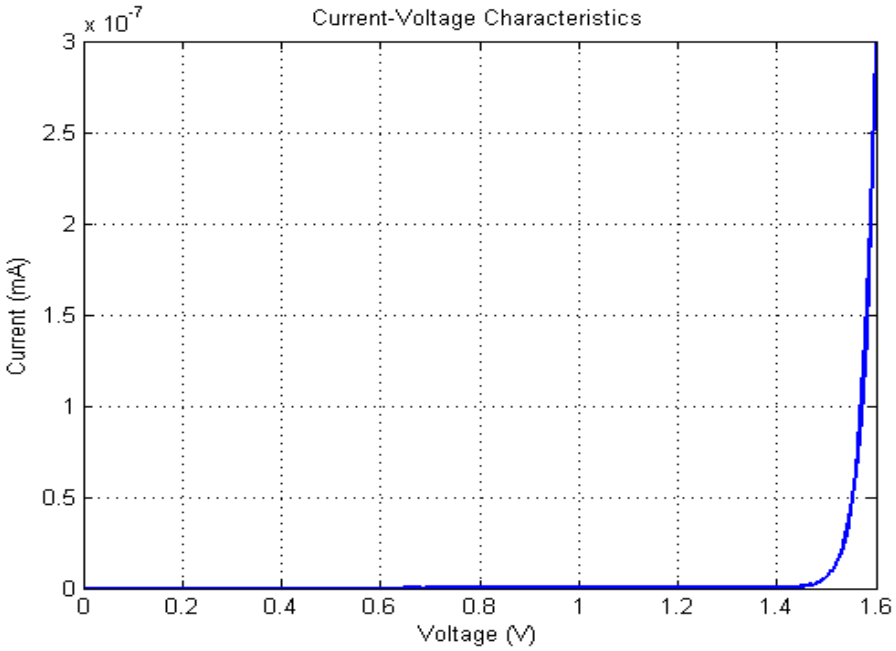

Figure 20 Current-Voltage Characteristics of CsPbBr3

The current-voltage (I-V) characteristic of a p-n junction was first developed by Shockley. For I-V curve of a p-n junction diode, the equation is referred by the Shockley equation. The Shockley equation for a diode with cross-sectional area A is

$$I = eA\left\langle \sqrt{\frac{D_p}{\tau_p}}\frac{n_i^2}{N_D} + \sqrt{\frac{D_n}{\tau_n}}\frac{n_i^2}{N_A}\right\rangle\left(e^{eV/kT} - 1\right)$$

The diode current saturates and the saturation current is given by the factor preceding the exponential function in the Shockley equation, under reverse bias conditions. The threshold voltage as well as the series resistance of the diode increases as the diode is cooled. If the device were driven at a constant voltage, a large current change would result from a change in temperature.

25. Band-Gap Energy as a Function of Temperature

The change in band-gap energy as a function of temperature is shown with the associated result figures. The eleven materials are tested for the band-gap as a function of temperature. In Figure.21, the band-gap energy is the main factor for the temperature dependence of diode voltage. The inspections of the figures reveal that the temperature increases, the energy gap of the semiconductors decreases. Therefore, the energy gap is time dependent for the materials of the device.

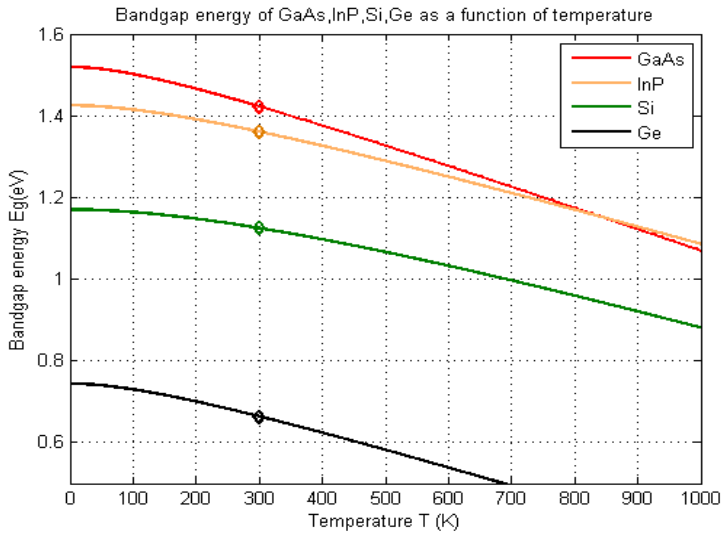

Figure 21 Band-Gap Energy of GaAs, InP, Si and Ge as a Function of Temperature

The band-gap energy of GaN and GaP as a function of temperature is shown in Figure 22 and 23. As the temperature increases, the energy band-gap of (GaN) gallium nitride and gallium phosphide (GaP) also decreases. Also, the band-gap energy of AlN, GaSb, InN, InAs and InSb as a function of temperature is shown in Figure.24.

As the temperature increases, the energy band-gap of (AlN) alluminium, (GaSb) gallium antimonide, (InN) indium nitride, (InAs) indium arsenide and (InSb) indium antimonide also decreases. Among the materials, indium antimonide (InSb) has the lowest energy band-gap.The energy band gap of semiconductors tends to decrease as the temperature is increased. This means that the interatomic spacing increases when the amplitude of the atomic vibrations increases due to the increased thermal energy. This effect is quantified by the linear expansion coefficient.

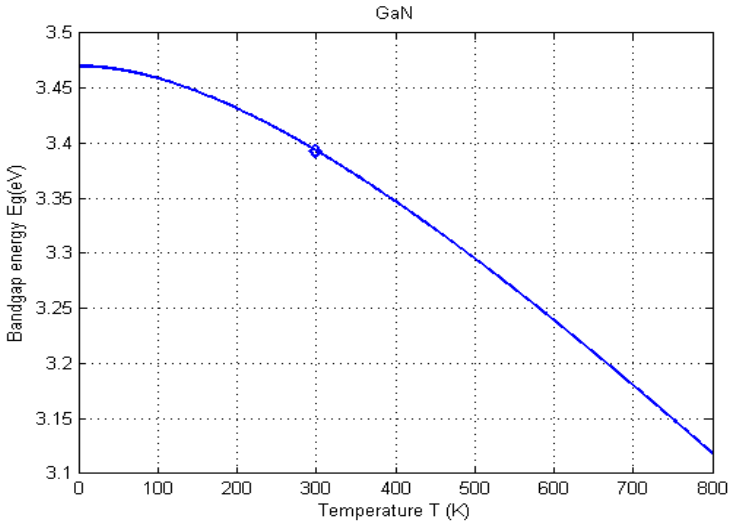

Figure 22 Band-Gap Energy of GaN as a Function of Temperature

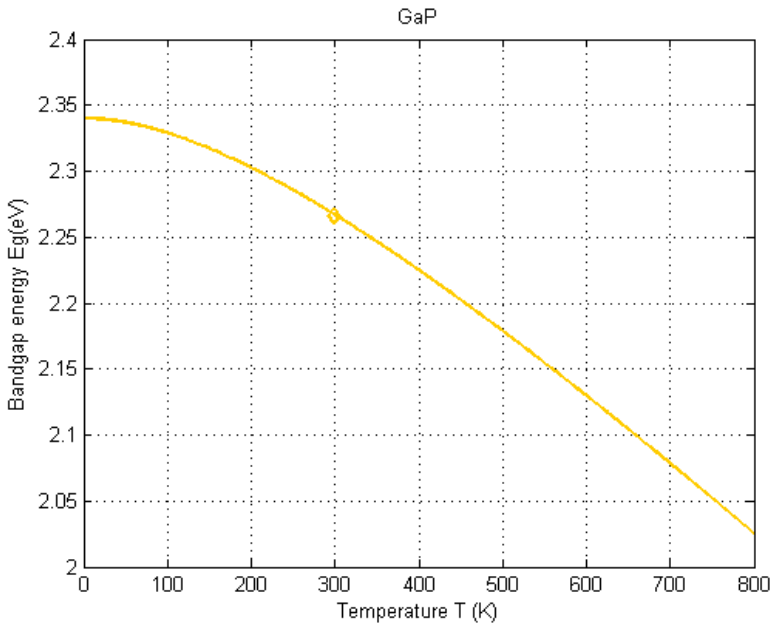

Figure 23 Band-Gap Energy of GaP as a Function of Temperature

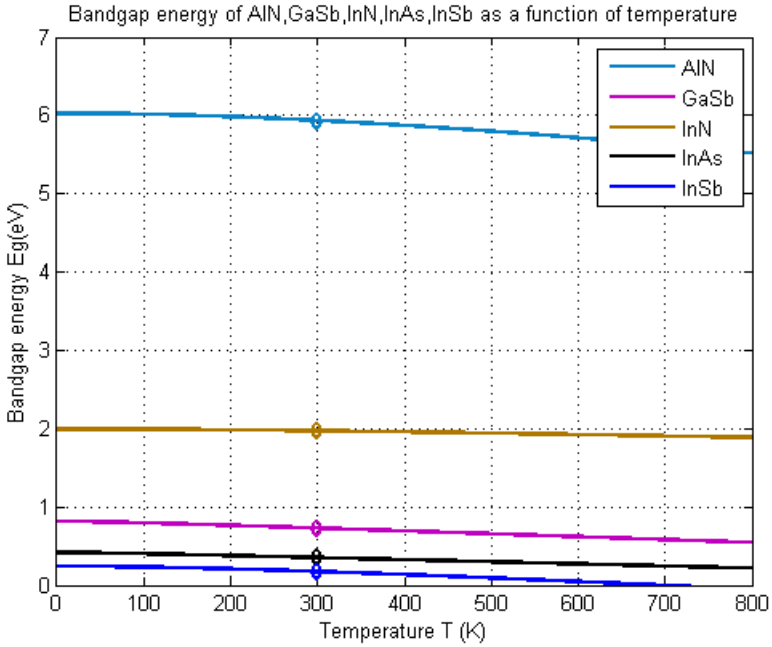

Figure 24 Band-Gap Energy of AlN, GaSb, InN, InAs and InSb as a Function of Temperature

26. Temperature Dependence of Emission Intensity

The result of the temperature dependence of the emission intensity are shown in Figure.25. The inspection of the figure reveals that the temperature dependence of the emission intensity at a constant current decreases with increasing temperature. This decrease of the emission intensity is

due to several temperature-dependent factors including (i) non-radiative recombination via deep levels, (ii) surface recombination, and (iii) carrier loss over heterostructure barriers.The temperature dependance of intensity is an important factor for light emitting diodes. When the temperature is high, the LED intensity drops. The temperature dependence of emission intensity is defined by the following equation.

$$I = I_{0K} \exp(-T/T_1)$$

where T_1 is the characteristic temperature that describes the temperature dependence of the LED.

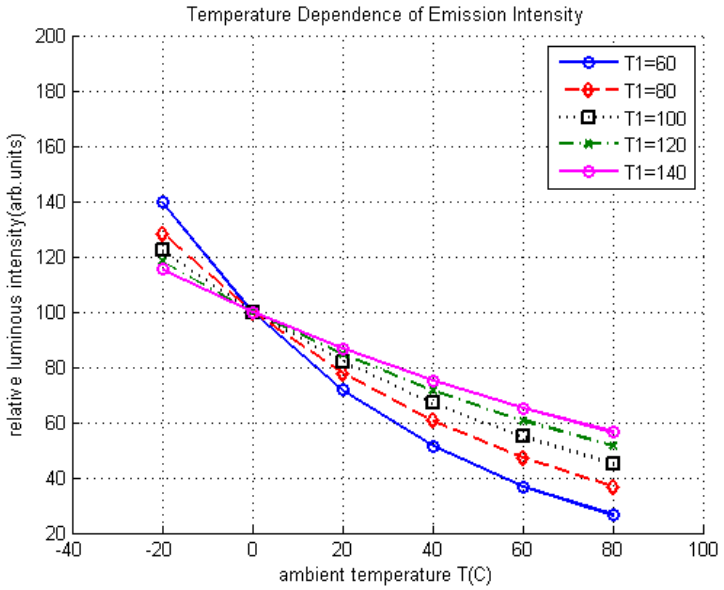

Figure 25 Temperature Dependence of Emission Intensity

27. Band Diagram of a p-GaAs/N-$Al_{0.3}Ga_{0.7}As$ Heterojunction

Figure 26 shows that a p-type narrow-gap semiconductor in contact with an N-type wide band-gap semiconductor of heterojunction. The Fermi level will line up to be a constant across the junction under thermal equilibrium conditions without any voltage bias, when the two crystals are in contact. The band structure plot is often first simplified in the form of a band diagram to know how band structure changes relative to the Fermi level. In a semiconductor, the Fermi level is surrounded by a band gap. The closest band above the band gap is called the conduction band and the closest band beneath the band gap is called the valence band.

As a result, the total width of the depletion region is 0.114 μm. The conduction band is very close to the Fermi level than the valence band. For p-type, the conduction band edge is 1367.6 meV. From the design of the band diagram, the conditions of the drift current or diffusion current flowing across the heterojunction can be observed. By analyzing the energy band structure, the effect of the forward voltage or barrier voltage can be observed, especially from the differences in energy gap.

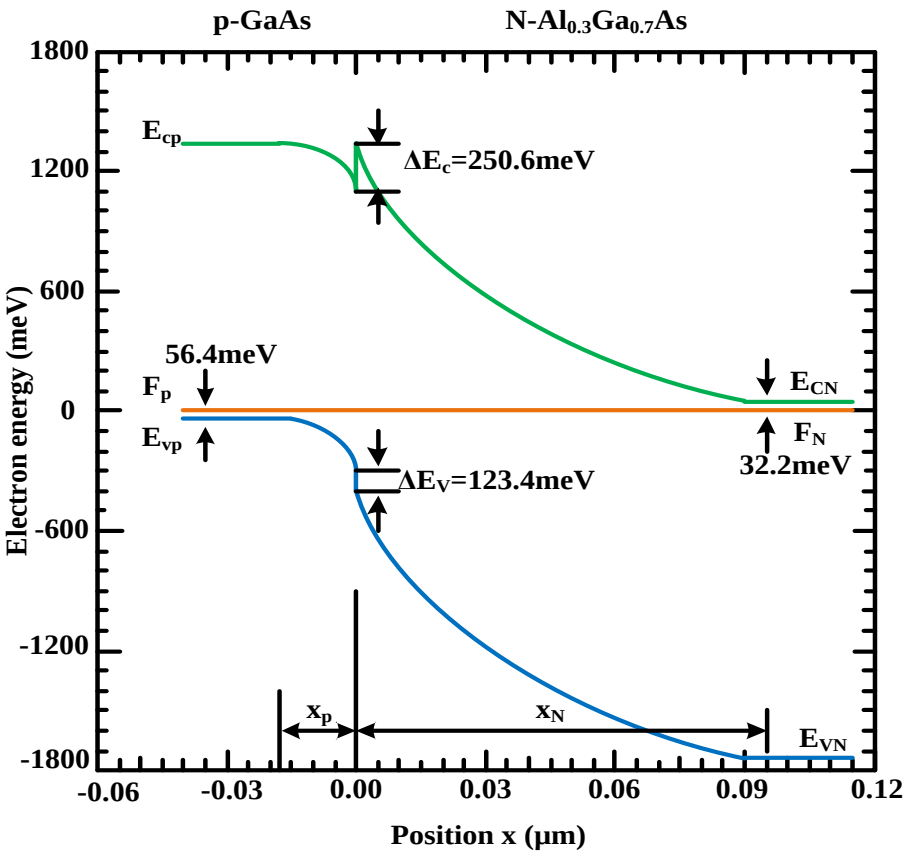

Figure 26 Band Diagram of a p-GaAs/N-Al0.3Ga0.7As Heterojunction

28. Band Diagram of n-GaAs/P-$Al_{0.3}Ga_{0.7}As$ Heterojunction

The band structure of semiconductor n-P heterojunction is shown in Figure.27. The step by step procedure to find the band diagram of n-P heterojunction is similar to that of the p-N heterojunction. The figure reveals that the wide-gap semiconductor is doped P-type and the narrow gap semiconductor is doped n-type. When the heterojunction is formed, a space charge region will exist due to the diffusion or redistribution of free carriers at thermal equilibrium. As a result, the total width of the depletion region is 0.24 μm and the conduction band is very close to the Fermi level than the valence band.

The n-N heterojunction theory is very useful for modeling high electron mobility transistors. However, depending on the model, the results may be different. The figure shows that the energy gap of P-type semiconductor is a little wider than n-type doped. The excess electrons on the n side near the junction may spill over the P side and the holes on the P side near the junction may spill over the n side.

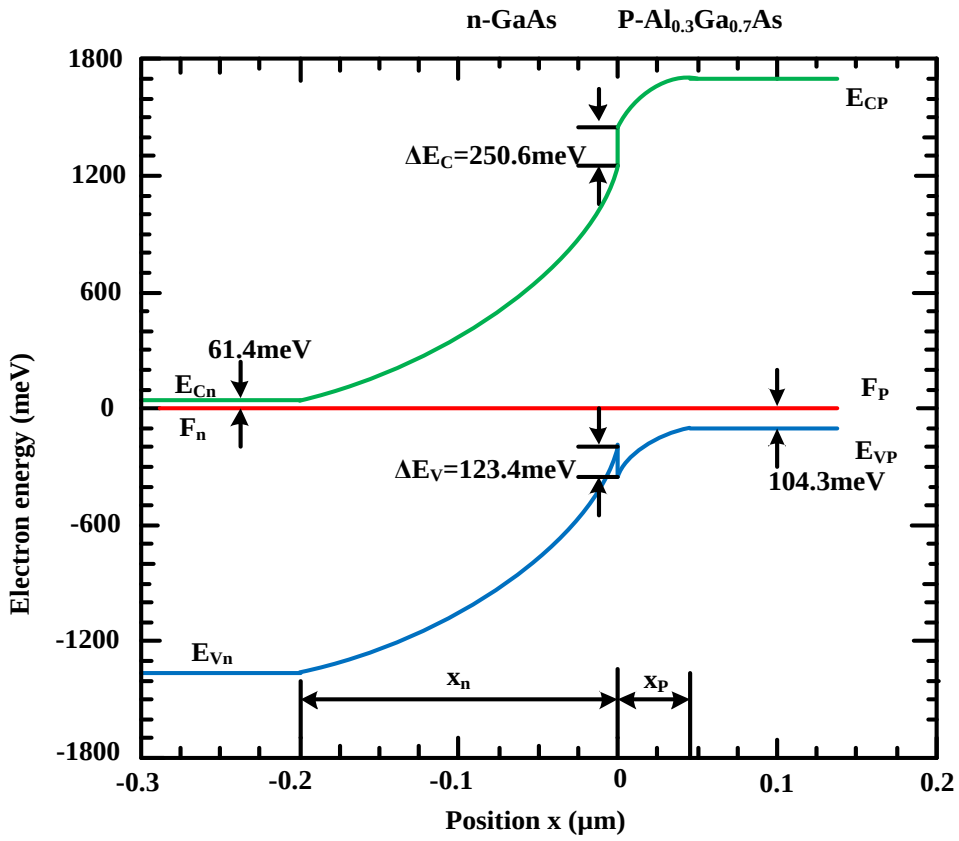

Figure 27 Band Diagram of an Unbiased n-GaAs/P-Al0.3Ga0.7As Heterojunction

29. Band Diagram of an Unbiased n-InN/P-GaN Heterojunction

The band structure of n-P heterojunction is shown in Figure.28. The step by step procedure to find the band diagram of n-P heterojunction is similar to that of the p-N heterojunction. The n-N heterojunction theory is very useful for modeling high electron mobility transistors. However, depending on the model, the results may be different. The figure shows that the energy gap of P-type semiconductor is a little wider than n-type doped. The excess electrons on the n side near the junction may spill over the P side and the holes on the P side near the junction may spill over the n side.

As a result, the total width of the depletion region is 0.06 μm and the conduction band is very close to the Fermi level than the valence band. The Fermi level will line up to be a constant across the junction under thermal equilibrium conditions without any voltage bias, when the two crystals are in contact. The conduction band edge discontinuities is 430meV and the valence band edge discontinuities is 1000meV.

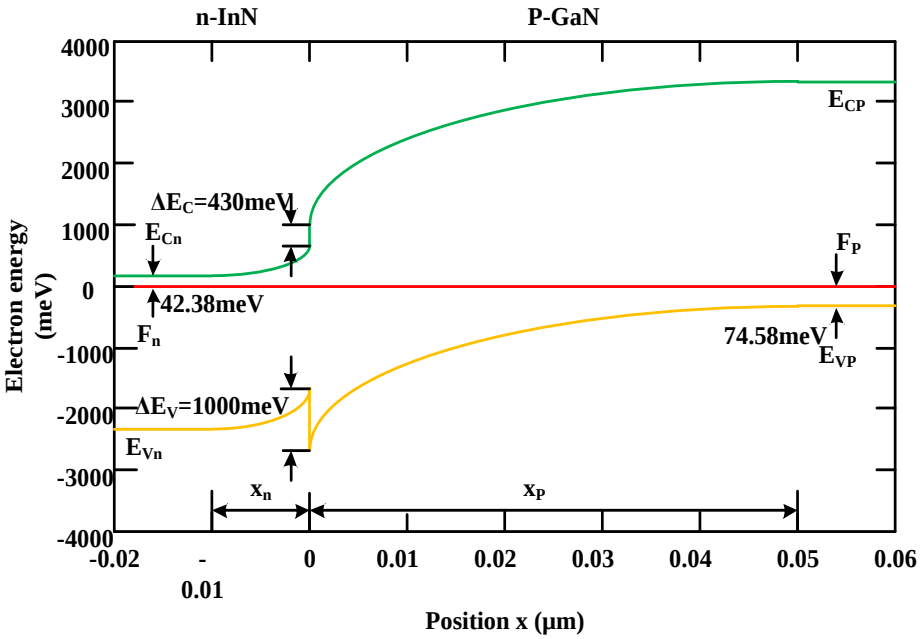

Figure 28 Band Diagram of an Unbiased n-InN/P-GaN Heterojunction

30. Band Diagram of a p-ZnCdO/N-ZnCdO Homojunction

The band diagram of p-ZnCdO/N-ZnCdO homojunction with $N_a=1x10^{17}$ cm^{-3} in the p region and $N_D=1x10^{18}$ cm^{-3} in the N region is shown in Figure.29. The procedure to design homojunction is similar to that of the heterojunction, except that there are no band edge discontinuities for both conduction and valence band.

The Fermi level will line up to be a constant across the junction under thermal equilibrium conditions without any voltage bias, when the two crystals are in contact. The conduction band edge is 2977meV. From this edge, the band decreases sharply 2679meV. Then, the band decreases slightly 268meV. A similar configuration can be observed for valence band. As a result, the total width of the depletion region is 0.17413 μm.

The conduction band is very close to the Fermi level than the valence band. The energy gap of the p-type doped and N-typed doped are nearly equal. There are no band edge discontinuities in p-ZnCdO/N-ZnCdO Homojunction. From the design of the band diagram, the conditions of drift current and diffusion current across the homojunction can be observed. Moreover, by analyzing the energy band structure, the effect of the forward voltage or barrier voltage can be observed, especially from the differences in energy gap.

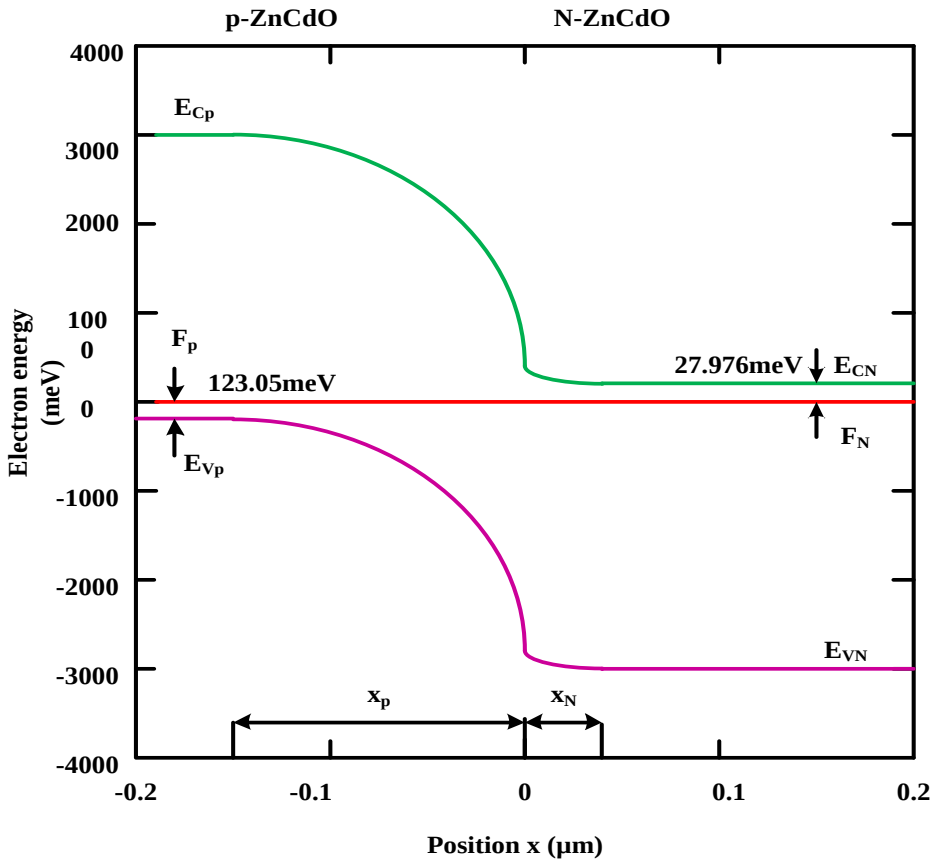

Figure 29 Band Diagram of a p-ZnCdO/N-ZnCdO Homojunction

31. Band Diagram of an Unbiased n-ZnO/P-$Al_{0.16}Ga_{0.84}N$ Heterojunction

The band structure of an unbiased n-ZnO/P-$Al_{0.16}Ga_{0.84}N$ heterojunctionis shown in Figure.30. The figure shows that the position of P-type semiconductor is larger than the n-type semiconductor. As a result, the total width of the depletion region is 0.4194 μm. The band edge discontinuities for conduction band is 133.678 meV and for valence band is 65.84 meV. The conduction band is very close to the Fermi level than the valence band.

The conduction band edge for P-type is obtained from the difference in the energy gap and the fermi level of the P-type material. Then, the band decrease according to the potential drop and finally close to the fermi level. A similar configuration can be occurred for valence band. From the design of the band diagram, the conditions of the drift current or diffusion current flowing across the heterjunction can be observed.

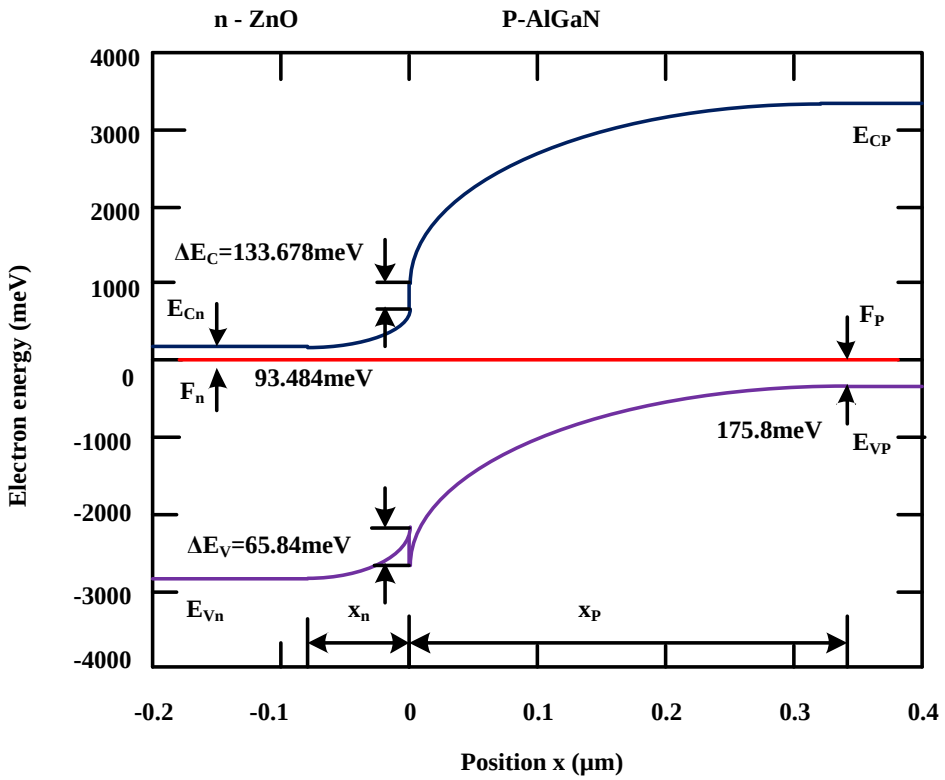

Figure 30 Band Diagram of an Unbiased n-ZnO/P-Al0.16Ga0.84N Heterojunction

32. Band Diagram of a p-Si/N-Si Homojunction

The band diagram of a p-Si /N-Sihomojunction with $N_a=3x10^{15}cm^{-3}$ in the p region and $N_D=1x10^{16}$ cm^{-3} in the N region is shown in Figure.31. As a result, the total width of the depletion region is 0.632 μm and the conduction band is close to the Fermi level than the valence band. The figure shows that the energy gap of p-type semiconductor is nearly equal to that of the N-type doped.

By analyzing the energy band structure, the effect of the forward voltage or barrier voltage can be observed, especially from the differences in energy gap. From the design of the band diagram, the conditions of the drift current or diffusion current can be observed.

The procedure to design homojunction is similar to that of the heterojunction, except that there are no band edge discontinuities for both conduction and valence band. The Fermi level will line up to be a constant across the junction under thermal equilibrium conditions without any voltage bias, when the two crystals are in contact. The effect of the forward voltage or barrier voltage can be observed.

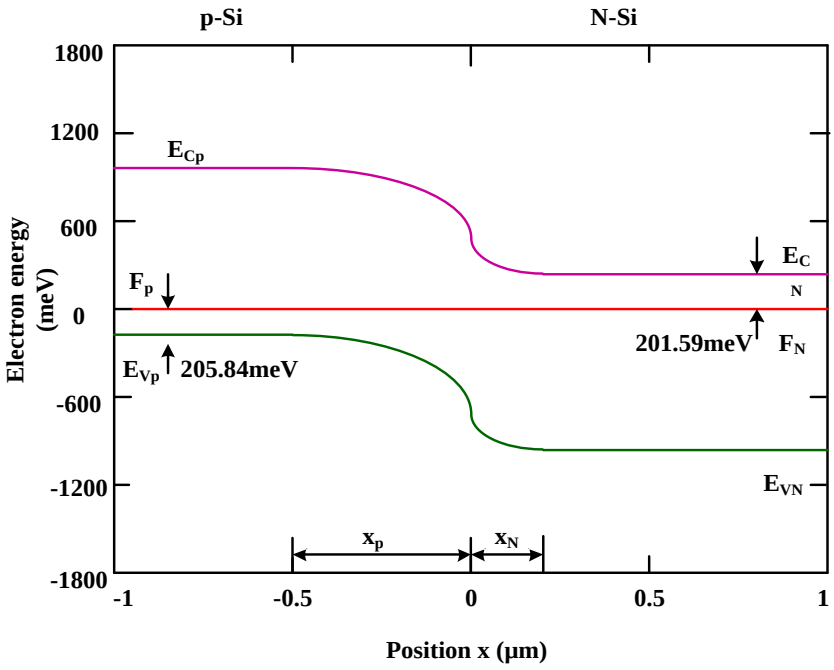

Figure 31 Band Diagram of a p-Si/N-Si Homojunction

33. Band Diagram of a p-Ge/N-Ge Homojunction

The band diagram of a p-Ge /N-Gehomojunction with $N_a=1x10^{16}cm^{-3}$ in the p region and $N_D=5x10^{13}$ cm^{-3} in the N region is shown in Figure.32.

As a result, the total width of the depletion region is 2.3115μm and the valence band is close to the Fermi level than the conduction band. The figure shows that the energy gap of p-type semiconductor is wider than that of the N-type doped. From the design of the band diagram, the conditions of the drift current or diffusion current flowing across the homojunction can be observed.

By analyzing the energy band structure, the effect of the forward voltage or barrier voltage can be observed, especially from the differences in energy gap. Moreover, the effect of the concentrations can be observed. The procedure to design homojunction is similar to that of the heterojunction, except that there are no band edge discontinuities for both conduction and valence band. The Fermi level will line up to be a constant across the junction under thermal equilibrium conditions without any voltage bias, when the two crystals are in contact. The effect of the forward voltage or barrier voltage can be observed.

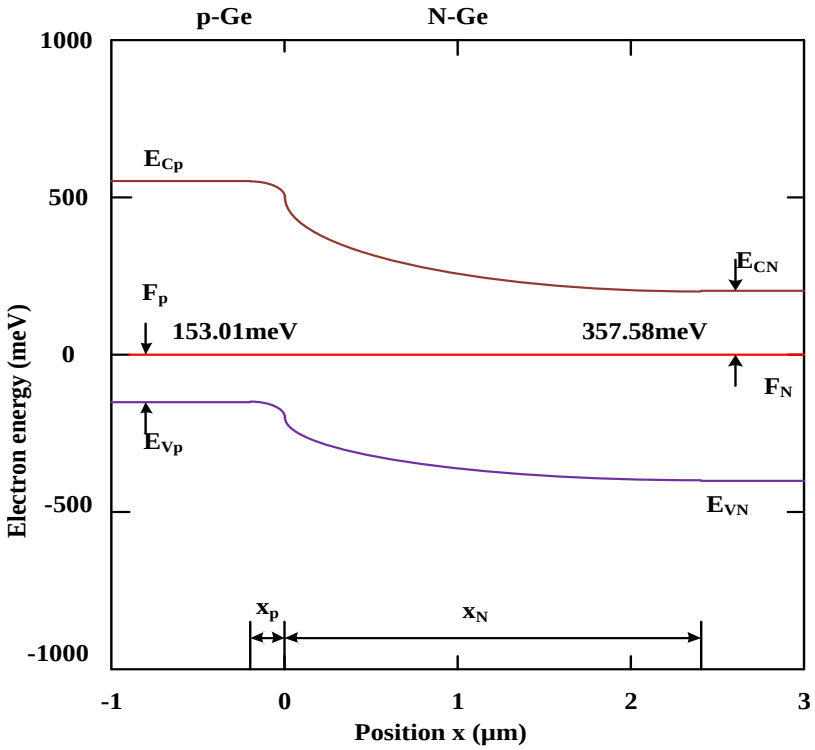

Figure 32 Band Diagram of a p-Ge/N-Ge Homojunction

34. Band Diagram of a p-$CsPbBr_3$ /N-$CsPbBr_3$ Homojunction

The band diagram of a p-$CsPbBr_3$ /N-$CsPbBr_3$ homojunction with $N_a=2x10^{18}cm^{-3}$ in the p region and $N_D=5x10^{17}$ cm^{-3} in the N region is shown in Figure.33. As a result, the total width of the depletion region is 0.0553μm and the valence band is close to the Fermi level than the conduction band. From the design of the band diagram, the conditions of the drift current or diffusion current flowing across the homojunction can be observed. By analyzing the energy band structure, the effect of the forward voltage or barrier voltage can be observed, especially from the differences in energy gap. Moreover, the effect of the concentrations can be observed. The procedure to design homojunction is similar to that of the heterojunction, except that there are no band edge discontinuities for both conduction and valence band.

The Fermi level will line up to be a constant across the junction under thermal equilibrium conditions without any voltage bias, when the two crystals are in contact. The effect of the forward voltage or barrier voltage can be observed by analyzing the energy band structure design.

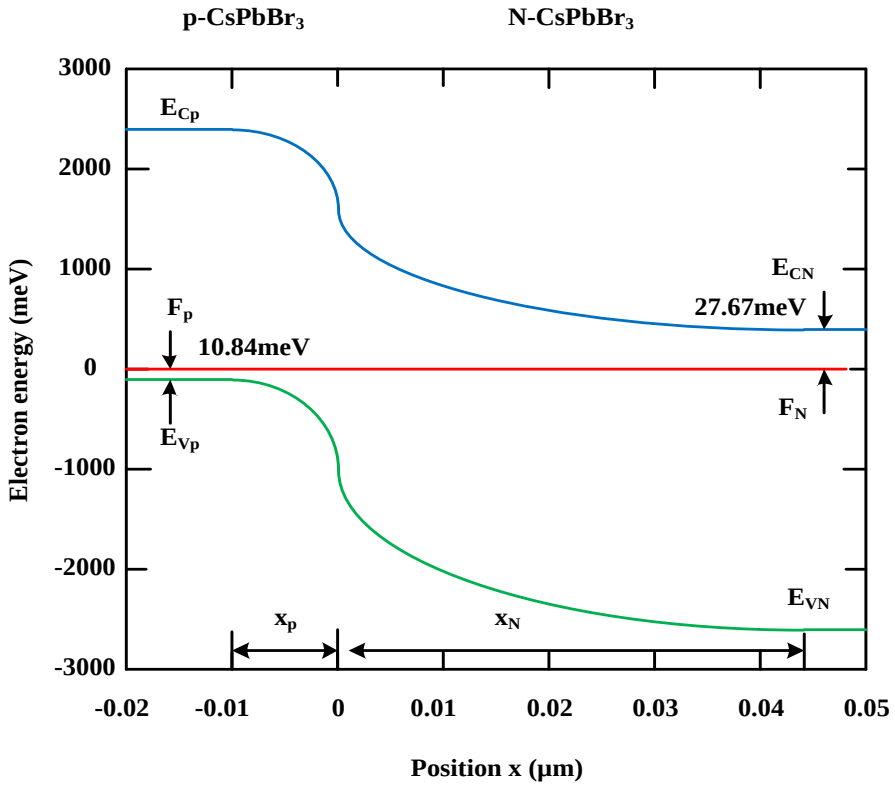

Figure 33 Band Diagram of a p-CsPbBr3 /N-CsPbBr3 Homojunction

35. Discussions and Conclusion

This research strongly focuses on the development the analysis of computer-based simulation design for light emitting diode modeling using the mathematical equations. Improving the efficiency of the light emitting diodes is a challenging work, especially in the case of nitride material system for LEDs. For each characteristic in this modeling, the appropriate algorithms are employed to obtain the good performance. In these studies the optical properties of the light emitting diodes are investigated. Detailed reports of the conditions have been discussed previously, and are summarized here for conclusion. The measurements using the characteristic equations are conducted for the electrical and optical characteristics of the device. Good electrical characteristics were observed for the design. This condition is the background for developing high quality devices.

The analytical results were compared with the experimental measurements. The external quantum efficiency of the LED was improved by the simulation results. The V-I characteristics of the LED devices are in good agreement with the properties of the materials used for the crystal growth. The research approves the existing system from the literature background. The current-voltage characteristics of the existing materials are mentioned, such as silicon and germanium. The band gap energy as a function of temperature for the materials such as gallium nitride, gallium phosphide, gallium arsenide, indium phosphide, silicon and germanium are briefly explained. From the results, it shows that the fundamental band-gap energy decreases when the temperature increases. Moreover, the temperature dependence of the emission intensity is discussed.

The band structures of semiconductors for Si, Ge, ZnCdO, $CsPbBr_3$, InN/GaN, ZnO/AlGaN, GaAs/AlGaAs are discussed with figures. The band diagrams are designed for both homojunctions and heterojunctions. The step by step procedure to find the homojunction is the same that of the heterojunction except that there are no band edge discontinuities for homojunction. Moreover, in homojunction of the energy band structure design, the energy gaps of the conduction band and the valence band are same for both type of the material. For p-GaAs/N-$Al_{0.3}Ga_{0.7}As$, n-GaAs/P-$Al_{0.3}Ga_{0.7}As$, n-InN/P-GaN, n-ZnO/P-$Al_{0.16}Ga_{0.84}N$, the conduction band is close to the Fermi level than the valence band. From the design of the band diagram, the conditions of the drift current or diffusion current flowing across the heterojunction can be observed. By analyzing the energy band structure, the effect of the forward voltage or barrier voltage can be observed, especially from the differences in energy gap. A p-type semiconductor is in contact with an N-type band-gap semiconductor or a n-type semiconductor is in contact with the P-type semiconductor. The Fermi level will line up to be a constant across the junction under thermal equilibrium conditions without any voltage bias, when the two crystals are in contact.

References

[1] H. C. Casey, Jr.: *Temperature Dependence of Threshold Current Density on InP-$Ga_{0.28}In_{0.72}As_{0.6}P_{0.4,}$ 1.3μm for Double Heterostructure Lasers*, J. Appl. Phys., vol56, no.7, pp. 1959-1964, 1984

[2] R. Binder, P. Blood & M. Osinski: *Physics and Simulation of Optoelectronic Devices VII*, SPIE Proc. 3944, 2000

[3] Ahrenkiel R. K.: *Minority-Carrier Lifetime in III-V Semiconductors in Minority Carriers in III-V Semiconductors: Physics and Applications,* edited by R. K. Ahrenkiel and M. S. Lundstrom Semiconductors and Semimetals Vol. 39, 40, Academic Press, San Diego, 1993

[4] Schubert E. F.: *Doping in III-V Semiconductors,* Cambridge University Press, Cambridge UK, 1993

[5] Olshansky R., Su C. B., Manning J., and Powazinik W.*: Measurement of Radiative and Non-Radiative Recombination Rates in InGaAsP and AlGaAs Light Sources*, IEEE J. Quantum Electronics QE-20, 838, 1984

[6] Pantelides S. T. (Editor): *Deep Centers in Semiconductors*, Gordon and Breach, Yverdon Switzerland, 1992

[7] Ebeling K. J.: *Integrated Opto-Electronics*, Springer, Berlin, 1993

[8] Emerson D., Abare A., Bergmann M., Slater D., and Edmond J.: *Development of Deep UV III-V Optical Sources*, 7th International Workshop on Wide-Bandgap III-Nitrides, Richmond V*A*, March ,2002

[9] Hunt N. E. J., Schubert E. F., Sivco D. L., Cho A. Y., and Zydzik G. J.: *Power and Efficiency Limits in Single-Mirror Light-Emitting Diodes with Enhanced Intensity*, Electronics Lett. 28, 2169, 1992

[10] Rhoderick E. H. and Williams R. H.: *Metal-Semiconductor Contacts*, Clarendon Press, Oxford, UK, 1988

[11] Schubert E. F., Tu L.-W., Zydzik G. J., Kopf R. F., Benvenuti A., and Pinto M. R.: *Elimination of Heterojunction Band Discontinuities by Modulation Doping*, Appl. Phys. Lett. 60, 466, 1992

[12] Sugawara H., Ishikawa M., Kokubun Y., Nishikawa Y., Naritsuka S., Itaya K., Hatakoshi G., Suzuki M.,: *Semiconductor Light Emitting Device*, US Patent 5,153,889, issued Oct. 6, 1992

[13] Krames M. R. et al.,: *High-Brightness AlGaInP Light-Emitting Diodes*, Proceedings of SPIE 3938, 2, 2000